Simultaneous Structural and Environmental Loading of an Ultra-High Performance Concrete Component

July 2010

NTIS Accession No. PB2010-110331

FHWA Publication No. FHWA-HRT-10-054

U.S. Department of Transportation
Federal Highway Administration

FOREWORD

With the ever increasing congestion and deterioration of our nation's highway system, a need exists to develop highly durable and rapidly constructed infrastructure systems. Durable bridge structures that would require less intrusive maintenance and would exhibit longer life spans thus maximizing the use of the facility are highly desirable. Expediting bridge construction can minimize traffic flow disruptions. Ultra-high performance concrete (UHPC) is an advanced construction material which affords new opportunities to envision the future of the highway infrastructure. The Federal Highway Administration has been engaged in research into the optimal uses of UHPC in the highway bridge infrastructure since 2001 through its Bridge of the Future initiative. This report presents results of a study aimed at assessing the performance of UHPC subjected to simultaneous structural and environmental loading. Although rarely investigated concurrently, this loading situation is commonly present in transportation structures. This research program demonstrates a feasible means to complete combined load testing. It also shows that UHPC is not exceptionally susceptible to environmentally-driven degradation when cyclically loaded past its elastic limit.

This report corresponds to the TechBrief titled, "Simultaneous Structural and Environmental Loading of an Ultra-High Performance Concrete Component" (FHWA-HRT-10-055). This report is being distributed through the National Technical Information Service for informational purposes. The content in this report is being distributed "as is" and may contain editorial or grammatical errors.

Quality Assurance Statement

The Federal Highway Administration (FHWA) provides high-quality information to serve Government, industry, and the public in a manner that promotes public understanding. Standards and policies are used to ensure and maximize the quality, objectivity, utility, and integrity of its information. FHWA periodically reviews quality issues and adjusts its programs and processes to ensure continuous quality improvement.

TECHNICAL REPORT DOCUMENTATION PAGE

1. Report No. FHWA-HRT-10-054	2. Government Accession No. NTIS PB2010-110331	3. Recipient's Catalog No.
4. Title and Subtitle Simultaneous Structural and Environmental Loading of an Ultra-High Performance Concrete Component		5. Report Date July 2010
		6. Performing Organization Code:
7. Author(s) Benjamin A. Graybeal		8. Performing Organization Report No.
9. Performing Organization Name and Address Office of Infrastructure Research & Development Federal Highway Administration 6300 Georgetown Pike McLean, VA 22101-2296		10. Work Unit No.
		11. Contract or Grant No.
12. Sponsoring Agency Name and Address Office of Infrastructure Research & Development Federal Highway Administration 6300 Georgetown Pike McLean, VA 22101-2296		13. Type of Report and Period Covered Final Report: 2009-2010
		14. Sponsoring Agency Code HRDI-06
15. Supplementary Notes		

16. Abstract

Ultra-high performance concrete (UHPC) is an advanced cementitious composite material which tends to exhibit superior properties such as increased durability, strength, and long-term stability. This experimental investigation focused on the flexural performance of a UHPC component subjected to a simultaneous combination of structural loading and aggressive environmental conditions. This situation is commonly present in transportation structures subjected to frequent transient loads and deicing chemicals. The UHPC component was cyclically loaded beyond its elastic limit in the presence of a 15% NaCl solution. Although UHPC tends to exhibit a larger number of small width, tightly spaced cracks, any ingress of liquids into the UHPC component along crack faces raises the possibility of steel fiber reinforcement degradation and a resulting loss of UHPC tensile capacity.

The simultaneous application of structural and environmental loadings to a UHPC flexural member did not result in any apparent degradation of the member's flexural capacity. The structural and environmental loading was conducted for 154 days during which 500,000 cycles were applied. NaCl solution ingress occurred, but no fiber reinforcement degradation was observed. Additionally, uniaxial tensile testing of UHPC prismatic sections was demonstrated as a viable means of assessing the tensile properties of this fiber-reinforced concrete.

This report corresponds to the TechBrief titled "Simultaneous Structural and Environmental Loading of an Ultra-High Performance Concrete Component" (FHWA-HRT-10-055).

17. Key Words	18. Distribution Statement
Ultra-high performance concrete, UHPC, fiber-reinforced concrete, bridges, accelerated construction, durable infrastructure systems, crack section permeability, simultaneous structural and environmental loading, NaCl solution.	No restrictions. This document is available through the National Technical Information Service, Springfield, VA 22161.

19. Security Classif. (of this report)	20. Security Classif. (of this page)	21. No. of Pages	22. Price
Unclassified	Unclassified	42	N/A

Form DOT F 1700.7 (8-72) Reproduction of completed page authorized

SI* (MODERN METRIC) CONVERSION FACTORS

APPROXIMATE CONVERSIONS TO SI UNITS

Symbol	When You Know	Multiply By	To Find	Symbol
		LENGTH		
in	inches	25.4	millimeters	mm
ft	feet	0.305	meters	m
yd	yards	0.914	meters	m
mi	miles	1.61	kilometers	km
		AREA		
in^2	square inches	645.2	square millimeters	mm^2
ft^2	square feet	0.093	square meters	m^2
yd^2	square yard	0.836	square meters	m^2
ac	acres	0.405	hectares	ha
mi^2	square miles	2.59	square kilometers	km^2
		VOLUME		
fl oz	fluid ounces	29.57	milliliters	mL
gal	gallons	3.785	liters	L
ft^3	cubic feet	0.028	cubic meters	m^3
yd^3	cubic yards	0.765	cubic meters	m^3
	NOTE: volumes greater than 1000 L shall be shown in m^3			
		MASS		
oz	ounces	28.35	grams	g
lb	pounds	0.454	kilograms	kg
T	short tons (2000 lb)	0.907	megagrams (or "metric ton")	Mg (or "t")
		TEMPERATURE (exact degrees)		
^oF	Fahrenheit	5 (F-32)/9 or (F-32)/1.8	Celsius	^oC
		ILLUMINATION		
fc	foot-candles	10.76	lux	lx
fl	foot-Lamberts	3.426	candela/m^2	cd/m^2
		FORCE and PRESSURE or STRESS		
lbf	poundforce	4.45	newtons	N
lbf/in^2	poundforce per square inch	6.89	kilopascals	kPa

APPROXIMATE CONVERSIONS FROM SI UNITS

Symbol	When You Know	Multiply By	To Find	Symbol
		LENGTH		
mm	millimeters	0.039	inches	in
m	meters	3.28	feet	ft
m	meters	1.09	yards	yd
km	kilometers	0.621	miles	mi
		AREA		
mm^2	square millimeters	0.0016	square inches	in^2
m^2	square meters	10.764	square feet	ft^2
m^2	square meters	1.195	square yards	yd^2
ha	hectares	2.47	acres	ac
km^2	square kilometers	0.386	square miles	mi^2
		VOLUME		
mL	milliliters	0.034	fluid ounces	fl oz
L	liters	0.264	gallons	gal
m^3	cubic meters	35.314	cubic feet	ft^3
m^3	cubic meters	1.307	cubic yards	yd^3
		MASS		
g	grams	0.035	ounces	oz
kg	kilograms	2.202	pounds	lb
Mg (or "t")	megagrams (or "metric ton")	1.103	short tons (2000 lb)	T
		TEMPERATURE (exact degrees)		
^oC	Celsius	1.8C+32	Fahrenheit	^oF
		ILLUMINATION		
lx	lux	0.0929	foot-candles	fc
cd/m^2	candela/m^2	0.2919	foot-Lamberts	fl
		FORCE and PRESSURE or STRESS		
N	newtons	0.225	poundforce	lbf
kPa	kilopascals	0.145	poundforce per square inch	lbf/in^2

*SI is the symbol for the International System of Units. Appropriate rounding should be made to comply with Section 4 of ASTM E380.
(Revised March 2003)

TABLE OF CONTENTS

LIST OF FIGURES

LIST OF TABLES

CHAPTER 1. INTRODUCTION

INTRODUCTION

Ultra-high performance concrete (UHPC) is an advanced cementitious composite material which has been developed in recent decades. When compared to more conventional cement-based concrete materials, UHPC tends to exhibit superior properties such as increased strength, durability, long-term stability.

This experimental investigation focused on the flexural performance of a UHPC component subjected to a simultaneous combination of structural loading and aggressive environmental conditions. Prior research studies have investigated the durability both of unloaded, uncracked UHPC and of unloaded, cracked UHPC[1]. However, in each case the ability of potentially deleterious liquids to travel through the UHPC would be reduced as compared to the case of a structural component that is cyclically loaded beyond its elastic limit while in an aggressive environment. This situation is commonly present in transportation structures subjected to frequent transient loads and deicing chemicals.

Structural cracking in UHPC components differs from the type of structural cracking observed in conventional concrete. UHPC tends to exhibit a larger number of small width, tightly spaced cracks[2,3,4]. Laboratory experience in this and other ongoing studies has demonstrated that crack widths between 2 and 8 micrometers (0.00008 and 0.00031 in.) are common[5].

In conventional concrete, small discontinuous cracks tending to surround aggregate particles are known as microcracks. These cracks have widths on the order of 10 to 100 micrometers[6]. Concrete cracks smaller than 40 to 50 micrometers (0.0016 to 0.002 in.) have been reported to have little impact on the permeability of conventional concrete[7,8], however, this lack of influence may be due to the discontinuous nature of microcracks in conventional concrete as opposed to the small width of the cracks.

UHPC exhibits little if any microcracking of the type distributed throughout conventional concretes, and correspondingly exhibits exceptionally low permeability when uncracked. However, it is anticipated that discrete structural cracking in UHPC components, even cracks of very small width, would necessarily increase the permeability. Even though these cracks would be of very small width, they may allow ingress of liquids into the UHPC component along crack faces thus raising the possibility of steel fiber reinforcement degradation and a resulting loss of UHPC tensile capacity.

OBJECTIVE

The objective of this research program was to evaluate the tensile response of UHPC subjected to simultaneous structural and environmental loading. The cyclic structural loading surpassed the elastic limit of the UHPC cementitious matrix, causing cracking of the concrete and potentially exposing the steel fiber reinforcement to a 15% concentration sodium chloride solution.

SUMMARY OF APPROACH

The research discussed herein focused on the cyclic loading of a UHPC beam, followed by a series of static tests intended to assess the tensile response of the UHPC. One mild steel reinforced, rectangular cross section UHPC beam spanning 4.88 m (16 feet) was fabricated. This beam was subjected to cyclic structural loading in a four-point bending configuration. The magnitude of load surpassed the elastic limit of the UHPC cementitious matrix, thus causing a series of flexural cracks to occur near midspan. The tensile face of the beam was subjected to continuous wetting via an open-cell sponge containing 15% sodium chloride solution.

The flexural performance of the beam was monitored for 154 days during which 500,000 cycles of structural load were applied. Afterward, the beam was loaded statically to flexural failure. Finally, a prism was cut from the bottom face of the beam near midspan and loaded in direct tension to failure. Each of these efforts was aimed at assessing the tensile performance of UHPC that had been subjected to structural fatigue loading in the presence of an environment that could potentially degrade the fiber reinforcement bridging tensile cracks.

OUTLINE OF REPORT

This report is divided into five chapters. Chapters 1 and 2 provide an introduction to the study and relate relevant background information necessary in understanding the study's results. Chapter 3 presents the geometric details of the UHPC beam along with the mechanical properties of the UHPC and mild steel reinforcement included in the study. Chapter 4 presents the test results and an analysis thereof. Finally, Chapter 5 presents the conclusions of this research program.

CHAPTER 2. BACKGROUND

INTRODUCTION

This chapter provides background information relevant to the focus of the research effort. A general discussion of UHPC constituent materials and material properties is presented.

UHPC CONSTITUENT MATERIALS

The specific UHPC investigated in this study is a product of a major worldwide construction materials manufacturer and supplier. It is currently the only product of this type that is widely available in the U.S. in the quantities necessary for large scale infrastructure applications. Table 1 provides a typical UHPC composition[(1)].

As reported in reference (1), the constituent material proportions were determined, in part, based on an optimization of the granular mixture. This method allows for a finely graded and highly homogeneous concrete matrix. Fine sand, generally between 150 and 600 micrometers (μm), is dimensionally the largest granular material. The next largest particle is cement with an average diameter of approximately 15 μm. Of similar size is the crushed quartz with an average diameter of 10 μm. The smallest particle, the silica fume, has a diameter small enough to fill the interstitial voids between the cement and the crushed quartz particles. Dimensionally, the largest constituent in the mix is the steel fiber reinforcement. In this study, the fibers in the mix had a diameter of 0.2 mm (0.008 inch), a length of 12.7 mm (0.5 inch), and a minimum tensile strength of 2600 MPa (377 ksi). The fibers were included in the mix at two percent by volume. Given the relative sizes of the sand and the fibers, the steel fibers are able to reinforce the concrete matrix on the micro level.

Table 1. Typical UHPC composition.

Material	Amount (kg/m^3 (lb/yd^3))	Percent by Weight
Portland Cement	712 (1,200)	28.5
Fine Sand	1,020 (1,720)	40.8
Silica Fume	231 (390)	9.3
Ground Quartz	211 (355)	8.4
Superplasticizer	30.7 (51.8)	1.2
Accelerator	30.0 (50.5)	1.2
Steel Fibers	156 (263)	6.2
Water	109 (184)	4.4

UHPC MATERIAL PROPERTIES

The research program associated with reference (1) addressed the materials properties of the UHPC investigated in this study. A brief summary of the relevant results is presented in Table 2. Note that, as with the beam tested in this study, these results pertain to UHPC subjected to a steam-treatment soon after the initial phase of curing has been completed.

Table 2. Typical steam-treated UHPC material properties.

Material Characteristic	Average Result
Compressive Strength (ASTM C39; 28-day strength)	193 MPa
Modulus of Elasticity (ASTM C469; 28-day modulus)	52.4 GPa
Split Cylinder Cracking Strength (ASTM C496)	11.7 MPa
Prism Flexure Cracking Strength (ASTM C1018; 305-mm span; corrected)	9.0 MPa
Mortar Briquette Cracking Strength (AASHTO T132)	8.3 MPa
Direct Tension Cracking Strength (Axial tensile load)	9.7–11.0 MPa
Prism Flexural Tensile Toughness (ASTM C1018; 305-mm span)	$I_{30} = 53$
Long-Term Creep Coefficient (ASTM C512; 77 MPa sustained load)	0.29
Long-Term Shrinkage (ASTM C157; initial reading after set)	766 microstrain
Total Shrinkage (Embedded vibrating wire gage)	850 microstrain
Coefficient of Thermal Expansion (AASHTO TP60–00)	15.6×10^{-6}
Chloride Ion Penetrability (ASTM C1202; 28-day test)	18 coulombs
Chloride Ion Permeability (AASHTO T259; 12.7-mm depth)	< 0.06 kg/m^3
Scaling Resistance (ASTM C672)	No Scaling
Abrasion Resistance (ASTM C944 w/ 2x weight on ground surface)	0.17 grams lost
Freeze-Thaw Resistance (ASTM C666A; 600 cycles)	RDM = 96%
Alkali-Silica Reaction (ASTM C1260; tested for 28 days)	Innocuous

1 MPa = 145 psi
1 kg/m^3 = 1.69 lb/yd^3
1 g = 0.035 ounce

CHAPTER 3. BEAM DESIGN, FABRICATION, AND MATERIAL PROPERTIES

INTRODUCTION

The physical details of the beam tested in this study are described in this chapter. Basic geometric details of the beam are described first, followed by details of the UHPC mix design, mixing, placing, and curing. The material properties of the UHPC in the beam were obtained through the testing of cylinders cast along side the beam. The tensile properties of the mild steel reinforcement were obtained through uniaxial tensile testing of bar samples. These material properties are reported at the conclusion of this chapter.

BEAM DESIGN

The specimen tested in this study was a mild steel reinforced, rectangular cross section beam. The cross section was 381-mm (15-inch) deep and 152-mm (6-inch) wide. The mild steel reinforcement consisted of two #4 bars located toward the bottom of the beam with a 35-mm (1-3/8-inch) clear cover. The rebar were chaired into place through the use of short lengths of slab bolsters oriented across the beam width. The bolsters were positioned so as to allow for a clear span of 1.83 m (72 inch) at midspan. The beam had an overall length of 5.13 m (16 feet 10 inch).

BEAM FABRICATION

This beam was fabricated in the Turner-Fairbank Highway Research Center's Structural Testing Laboratory. The UHPC mixing, UHPC placing, and the beam curing all took place within the confines of the lab. The beam reported upon herein was cast just after the conclusion of the casting of 16 mild steel reinforced UHPC beams and 23 prestressed UHPC beams that were produced for use in parallel studies. As such, the processes implemented during the fabrication were well practiced and were completed without any difficulty.

The UHPC mix design included a very low water-to-cementitious materials ratio and 2% steel fiber reinforcement by volume. The mix proportions are shown in Table 3. The superplasticizer was Chryso® Fluid Premia 150. The accelerator was Rheocrete® CNI. The fibers included in the UHPC were undeformed cylindrical steel fibers.

Table 3. UHPC mix proportions.

Constituent	Weight per Volume, kg/m^3 (lb/yd^3)
Premix	2195 (3699)
Superplasticizer	30 (51)
Accelerator	26 (43)
Steel Fibers	156 (263)
Water	112 (189)

The UHPC was mixed in an Imer® Mortarman 750 portable pan mixer. The batch size was 0.16 m^3 (5.65 ft^3). The following steps were implemented during the mixing. First, the dry premix was placed in the mixer and briefly mixed. The water, to which half of the superplasticizer had been added, was then dispersed into the mixing UHPC. Four minutes later the remaining superplasticizer was dispersed into the mixer. Four minutes thereafter the accelerator was added to the mix. Fiber addition was initiated eighteen minutes after the initial water addition when the UHPC had reached a flowable condition. Over the course of two minutes all of the fibers were added to the mix. The fresh UHPC was discharged from the mixer beginning twenty-one minutes after initial water addition.

Given the capacity of the mixer and the volume of UHPC required, two separate batches needed to be mixed for the casting of the beam. After the conclusion of the mixing of the first batch, it was discharged into a 208-liter (55-gallon) barrel for temporary storage until the mixing of the second batch was nearly complete. Figure 1 shows the mixer discharging into the barrel. During the mixing of the second batch, the barrel lid was installed and the barrel was suspended from an overhead crane. The barrel was periodically rotated end-over-end so as to ensure that the exposed surface of the UHPC contained inside was frequently disturbed and did not dehydrate.

The formwork for the beam was composed of steel channel sections bolted together to form an open-topped box. The UHPC was placed into the form at one end of the beam and allowed to flow toward the other end. The UHPC was agitated during placement by form-mounted vibrators. The first batch of UHPC was placed into the form as the mixing of the second batch was being completed. Figure 2 shows the UHPC being poured from the barrel into the form and flowing along the length of the beam. Once the barrel had been fully discharged, the second batch of UHPC was discharged directly from the mixer into the form. Given the self-consolidating nature of UHPC, it can be assumed that most of the concrete in the lower half of the beam was composed of the first batch of UHPC. As is recognized to be the case for fiber-reinforced concrete, the casting technique employed here is recognized to preferentially orient the fiber reinforcement along the axis of the beam.

After the form had been filled, sheet plastic was placed on the exposed UHPC surface. Dimensional lumber was then placed over the plastic and clamped into place. This process was intended to limit potential dehydration of any exposed UHPC surface.

The beam form was stripped approximately two days after casting. Approximately one week after casting the beam was subjected to a steam treatment intended to enhance the material properties of the UHPC. The beam was placed in a steam chamber into which live steam was pumped. The temperature in the chamber was held above 95ºC for 48 hours. After the conclusion of the steam treatment, the beam was stored for six months prior to the initiation of testing.

Figure 1. Photo. Discharge of UHPC holding barrel.

Figure 2. Photo. Placement of UHPC into beam form.

UHPC MATERIAL PROPERTIES

During the placing of the two UHPC batches into the beam form, 76-mm (3-inch) and 102-mm (4-inch) diameter cylinder specimens were cast in order to allow for material property characterization. These cylinders were cast in the laboratory using concrete captured from the UHPC stream as it was dropping into the beam form. After casting, the cylinders were stored with the beam during curing and steam treatment.

The cylinders were prepared for testing by grinding both ends to create parallel surfaces through the use of a fixed end grinder. After preparation, the cylinders exhibited length to diameter ratios of approximately 1.9. Three tests were carried out on the cylinders, namely density, compressive strength, and split cylinder tensile strength. Density measurements were obtained through conventional means by measuring weight of each cylinder and dividing by the volume. The average density of the UHPC was 2515 kg/m^3 (157 lb/ft^3).

The compressive strength tests were completed according to ASTM C39[(9)], except that the load rate was increased to 1 MPa/sec (150 psi/sec). The compressive strength results are presented in Table 4. The tests were completed thirteen months after casting of the beam, which was near the conclusion of the cyclic flexural testing. Overall, the compressive strength of the UHPC used in the beam was approximately 214 MPa (31 ksi).

Table 4. Cylinder density and compressive strength test results.

Batch Placement into Form	Cylinder Number	Density, kg/m^3 (lb/ft^3)	Compressive Strength, MPa (ksi)
First	1	2518 (157.2)	221 (32.0)
First	2	2515 (157.0)	219 (31.8)
First	3	2520 (157.3)	210 (30.5)
Second	1	2508 (156.6)	210 (30.4)
Second	2	2505 (156.4)	215 (31.2)

The split cylinder tensile strength tests were completed according to the procedure described briefly in reference (1) and more fully in reference (10). The procedure is the same as that described in ASTM C496[(11)] with the exception of an increased load rate (3.45 MPa/min (500 psi/min)) and extra data collection allowing for determination of lateral specimen expansion throughout the test. A single 102-mm (4-inch) diameter cylinder was tested from each of the two concrete mixes placed into the beam form. The tests were completed thirteen months after casting. Results from these tests are presented in Table 5. The cracking tensile strength was approximately 9.7 MPa (1.4 ksi).

Table 5. Split cylinder tensile test results.

Batch Placement into Form	Cylinder Number	Cracking Strength, MPa (ksi)	Peak Strength, MPa (ksi)
First	1	10.1 (1.47)	23.2 (3.36)
Second	1	9.1 (1.32)	23.8 (3.45)

MILD STEEL REINFORCEMENT TENSILE PROPERTIES

Two #4 mild steel reinforcing bars, 5.03 m (198 inch) in length, were included as discrete flexural reinforcement along the length of the beam. Sample specimens were cut from overlength portions of each of these bars and tested in uniaxial tension according to ASTM A370[(12)]. The yield strengths of the steel were determined to be 460 and 481 MPa (66.7 and 69.8 ksi) for the two bars based on the 0.2% offset method. The ultimate strengths were 731 and 742 MPa (106.0 and 107.6 ksi). At failure, the elongations over an initial gage length of 200 mm (7.88 inch) were 14.7% and 11.3%. Figure 3 shows the stress-strain response from the first bar while Figure 4 shows the response from the second bar. Note that the stress is based on the nominal cross section of the bar and thus represents engineering stress. Additionally, note that the strain was calculated through readings captured by an extensometer placed on the bar up through a strain of approximately 0.02, after which the extensometer was removed and the machine cross-head displacement readings were used.

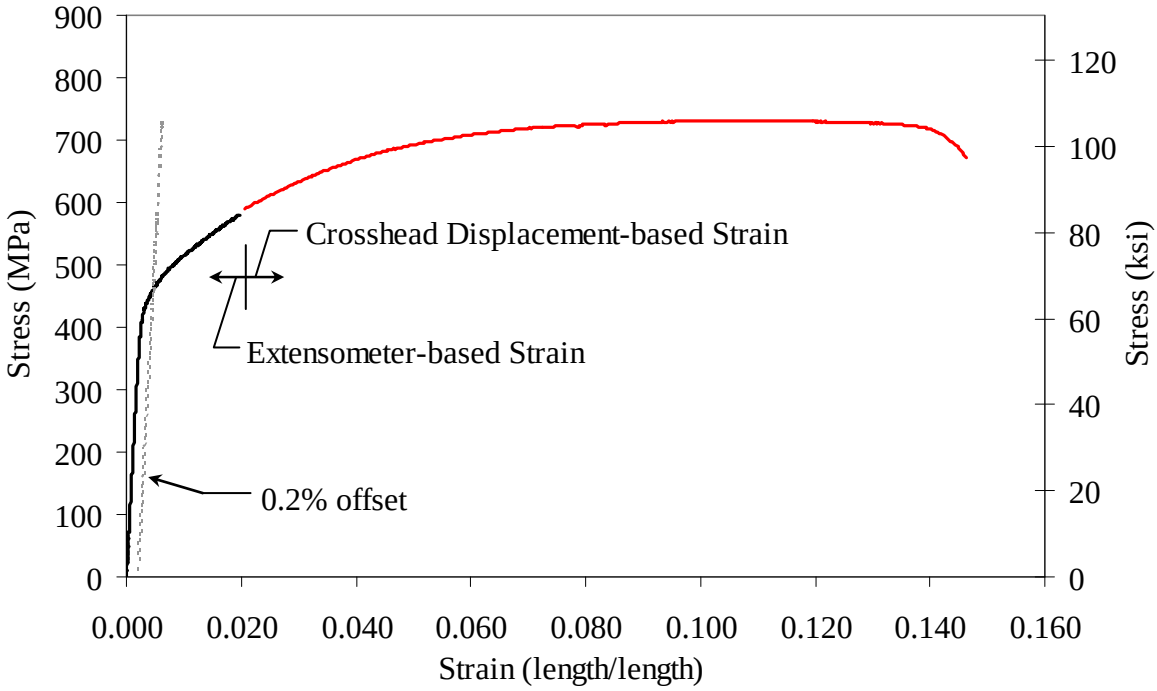

Figure 3. Graph. Tensile stress-strain response of first mild steel reinforcing bar.

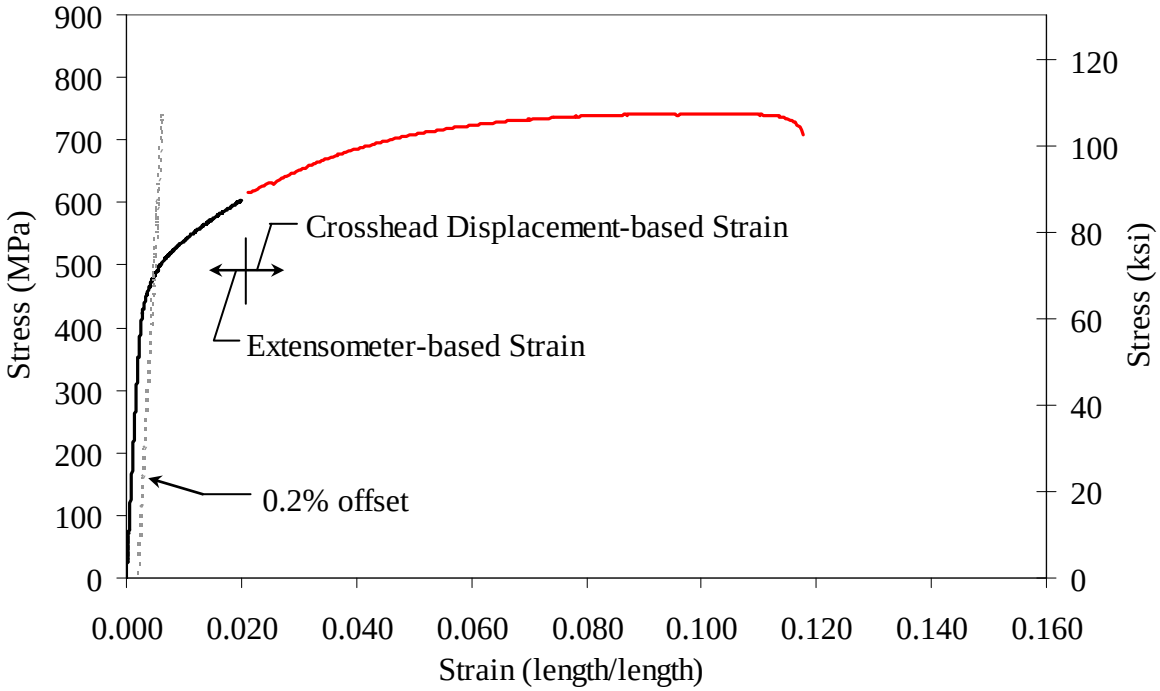

Figure 4. Graph. Tensile stress-strain response of second mild steel reinforcing bar.

CHAPTER 4. TESTING AND ANALYSIS OF RESULTS

INTRODUCTION

The experimental test program and the analysis of results are presented in this chapter. The cyclic flexural testing of the beam is discussed first. The results from the static flexural testing follow. Finally, the discussion of the uniaxial tension testing on an extracted prism is presented.

CYCLIC FLEXURAL TESTING OF BEAM

Test Setup

The cyclic flexural testing of this beam was completed through the use of a four-point bending test setup. The overall span of the beam was 4.88 m (16 ft) from center to center of roller support. Above and below the support rollers were approximately 25-mm (1-inch) thick concave steel plates. The load was applied to the beam through the use of a single servo-hydraulic jack centered over midspan of the beam. The jack loaded a 305-mm (12-inch) deep double-channel steel beam which in turn loaded two rollers that were sitting on steel plates above the beam. The 1.52-m (60-inch) distance between the centers of the load points created a constant applied moment region of the same length in the center of the span. The steel plates on which the load rollers sat were 152-mm (6-inch) wide and spanned across the top surface of the beam. These steel plates were grouted to the top surface of the beam prior to the start of loading. Figure 5 provides a photograph showing the loading arrangement for the cyclic testing of this beam.

The cyclic testing was conducted in three phases. The first was designed to allow for the observation of the initial flexural cracking of the beam. A structural load following a sinusoidal waveform at a frequency of 0.5 Hz was applied to the beam. The load range initially was 8.9 to 44.5 kN (2 to 10 kips). The peak load was incrementally increased to 53.4, 57.8, and 62.3 kN (12, 13, and 14 kips) after approximately 20 cycles at each load level. This phase was ceased when first flexural cracking was observed.

The second phase included the application of 1,000 cycles of structural loading onto the cracked beam. The cyclic structural load applied by the actuator followed a sinusoidal waveform with a frequency of 0.5 Hz over a load range from 8.9 to 71.2 kN (2 to 16 kips). After 100 cycles, the frequency was increased to 1.0 Hz.

After this phase was complete, the third phase was initiated. In this phase, the cyclic structural load again followed a sinusoidal waveform with a range of 8.9 to 71.2 kN (2 to 16 kips). The loading was programmed to apply a single sinusoidal cycle at a 1.0 Hz frequency taking the load from 8.9 kN (2 kips) to 71.2 kN (16 kips) then returning it to 8.9 kN (2 kips) where it would be held for the next 29 seconds. This loading program allowed for a 30 second total cycle time. In conjunction with this structural cyclic loading, an environmental loading component was added to concurrently act on the beam. The environmental load consisted of the application of a 15% concentration NaCl solution to the tensile face of the beam. This solution was applied to the beam through an open-cell foam pad which rested in a tray containing the salt solution. The foam was situated so that it was slightly compressed when the applied load was removed from the beam, and was further compressed in the applied structural cyclic load range of 8.9 to

71.2 kN (2 to 16 kips). The total length of the foam was 0.89 m (35 inches), thus the tensile face of the beam was subjected to this environmental loading over this distance centered on midspan. Figure 6 provides a photograph of salt solution application system immediately after its insertion under the beam. The combined structural and environmental loading was continued for a total of 499,000 total structural loading cycles which were completed over a time period of 154 days.

Figure 5. Photo. Four-point bending test setup for cyclic flexural load application.

Figure 6. Photo. Salt water solution application system.

Instrumentation and Observation Techniques

The cyclic behavior of the beam was assessed through a variety of techniques. Load and displacement were monitored through the hydraulic actuator's internal load cell and LVDT. Propagation of the salt solution along flexural cracks was monitored through visual observation of salt deposits on the vertical faces of the beam. Finally, crack locations and sizes on the tensile face of the beam were assessed through the use of a digital optical microscope mounted on a linear traverse system. This system was used to assess the cracks on the bottom face of the beam along the beam midline within 0.51 m (20 inches) of midspan. Figure 7 provides a photograph of the crack assessment setup including the microscope head, the associated digital display and computer control system, and the linear traverse system. This crack assessment setup with its 200x to 1000x variable power microscope was capable of identifying, sizing, and photographing cracks as small as 2-μm (0.000079-inch) wide.

Figure 7. Photo. Crack assessment microscope and linear traverse system.

Test Results

First Flexural Cracking

As described above, the cyclic testing of the beam was completed in three phases. The first phase focused on determining the flexural cracking load of the beam. The relatively high tensile strength of UHPC combined with its comparatively homogeneous composition allowed for first cracking of the beam to be monitored through auditory observations. The 20 load cycles

completed between the applied load range of 8.9 and 44.5 kN (2 and 10 kips) did not result in any flexural cracking. Flexural cracks also did not occur over the load range between 8.9 and 53.4 kN (2 and 12 kips) or between 8.9 and 57.8 kN (2 and 13 kips). The first flexural crack was observed on the 12^{th} cycle between the loads of 8.9 and 62.3 kN (2 and 14 kips). One further cycle over this load range was completed during which the actuator load and displacement responses were captured, after which this phase of the cyclic testing was completed.

An elastic analysis was completed to determine the stresses in the constant moment region of the beam at first cracking. The dead load moment was 4.3 kN-m (38 kip-inches) and the applied moment at 62.3 kN (14 kips) of load was 52.2 kN-m (462 kip-inches), resulting in a total moment of 56.5 kN-m (500 kip-inches). Elastic properties of the midspan cross section were calculated to include a moment of inertia of 7.17×10^8 mm^4 (1722 in^4) and a centroid depth of 193 mm (7.57 inch) from the top of the beam. The elastic analysis indicates that the flexural tensile stress on the tensile face of the beam was 14.9 MPa (2.16 ksi) at first cracking.

Note that this first cracking flexural tensile strength of the UHPC is influenced by the casting techniques employed. As has been recognized in the French UHPFRC Design Guideline[13] and has been reported in studies such as references (5, 14, and 15), preferential fiber alignment in the direction of casting flow and along formed surfaces can increase the tensile strength of these types of concrete.

Generation of a Set of Flexural Cracks

The second phase of the cyclic testing focused of the generation of a stable set of flexural cracks on the tensile face near midspan of the beam. This was accomplished by applying 1000 cycles of load over the range of 8.9 to 71.2 kN (2 to 16 kips). Given that the 71.2 kN (16 kip) load generated a moment 13% above the flexural cracking moment, it was anticipated that these load cycles would generate multiple tightly spaced flexural cracks as is common in discretely reinforced UHPC flexural members loaded beyond cracking[2,3,4]. As expected, within the first few dozen cycles additional flexural cracks were audibly observed to occur on cycles 1, 3, 4, 5, 8, 15, and 22.

Actuator load and displacement data were collected periodically throughout this phase of the cyclic testing. Figure 8 shows these results at six specific cycles including the cycle which caused first flexural cracking. The solid lines in the figure represent portions of each cycle where the load was increasing; the dotted lines represent decreasing load in the same cycle. This figure demonstrates that there was a detectable change in response between first cracking and each of the subsequent cycles shown. It also demonstrates that the majority of the change in response occurred within the first 31 cycles, indicating that the majority of the crack initiation/propagation occurred within these cycles.

An alternate means to assess the change in flexural response over the cycles completed in this phase of testing is to focus on the slope of the load-displacement response. The slope was calculated on the increasing load portion of each recorded cycle between the loads of 13.3 kN (3 kips) and 57.8 kN (13 kips). These results are plotted in Figure 9. This plot again illustrates how the majority of the change in response occurred within the first 31 cycles.

The flexural cracking of the beam was assessed following the completion of this phase of loading. The crack assessment system described above was used to quantify the cracks present along the midline of the bottom face of the beam within 508 mm (20 inches) of midspan. Each identified crack was noted for its location and width. Figure 10 displays the pertinent information on the 29 cracks identified. A total of 26 of these cracks fell within the region which would subsequently be subjected to the aggressive environment. These 26 cracks had an average width of 4.4 μm (0.00017 in.) with a standard deviation of 2.2 μm (0.000087 in.). Eight of these cracks exhibited widths greater than 6 μm (0.00024 in.). Figure 11 provides three photographs of cracks identified within the area to be subjected to the aggressive environment. Of note, the 8-μm (0.0003-in.) wide crack shown in Figure 11c is the widest observed crack within the portion of the bottom face of the beam to which the aggressive environment was applied.

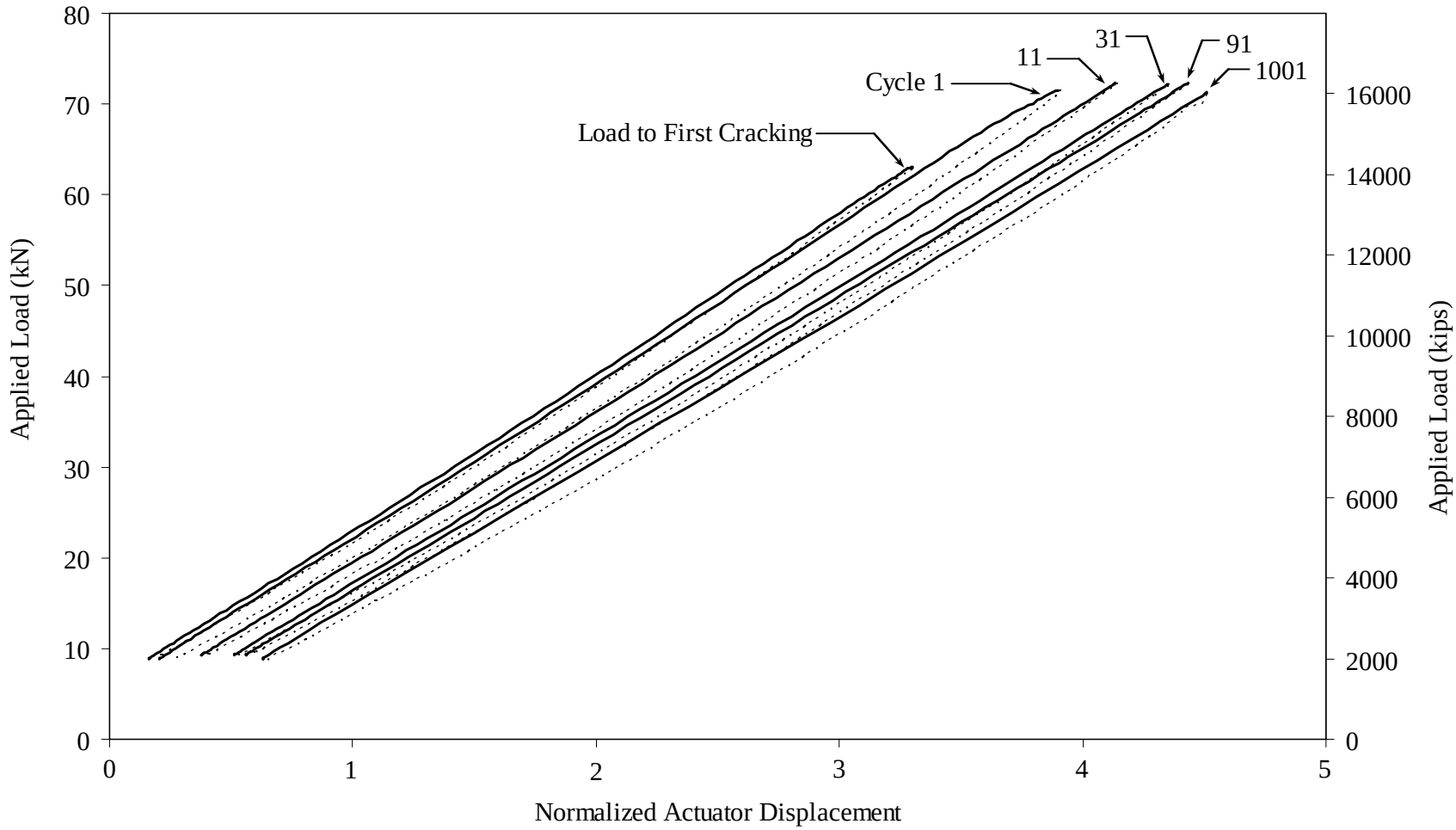

Figure 8. Graph. Actuator load versus displacement response during second phase of cyclic loading.

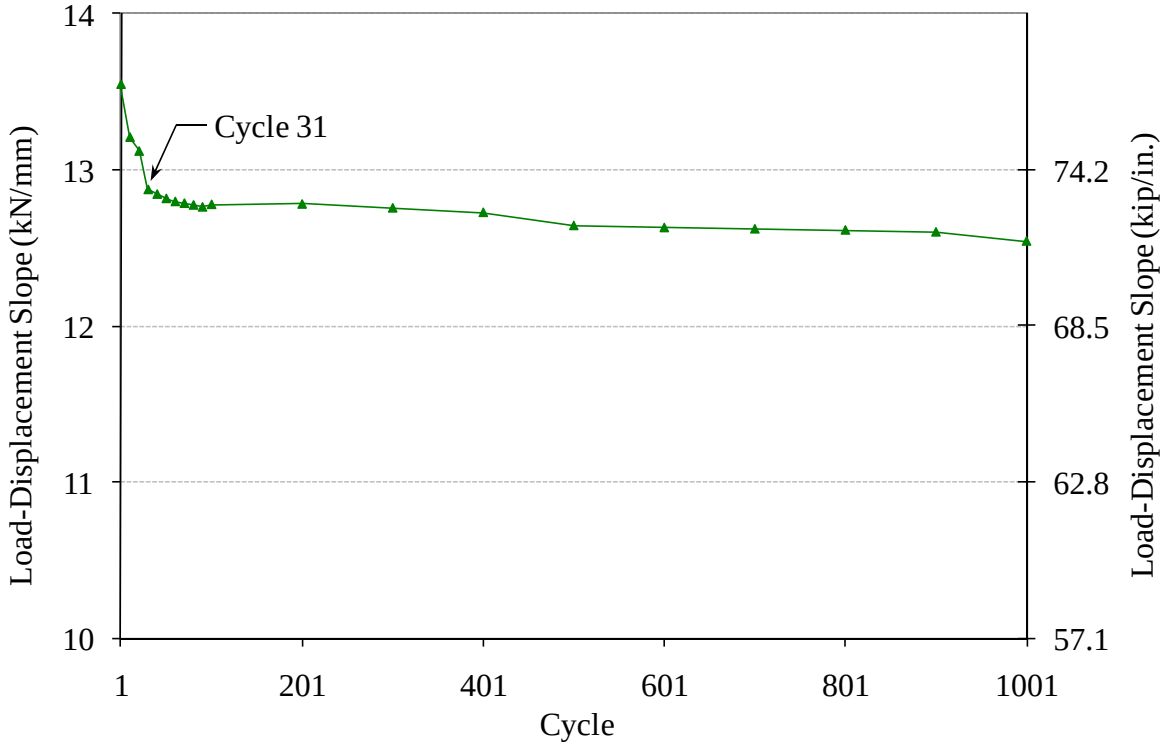

Figure 9. Graph. Actuator load-displacement response slope during second phase of cyclic loading.

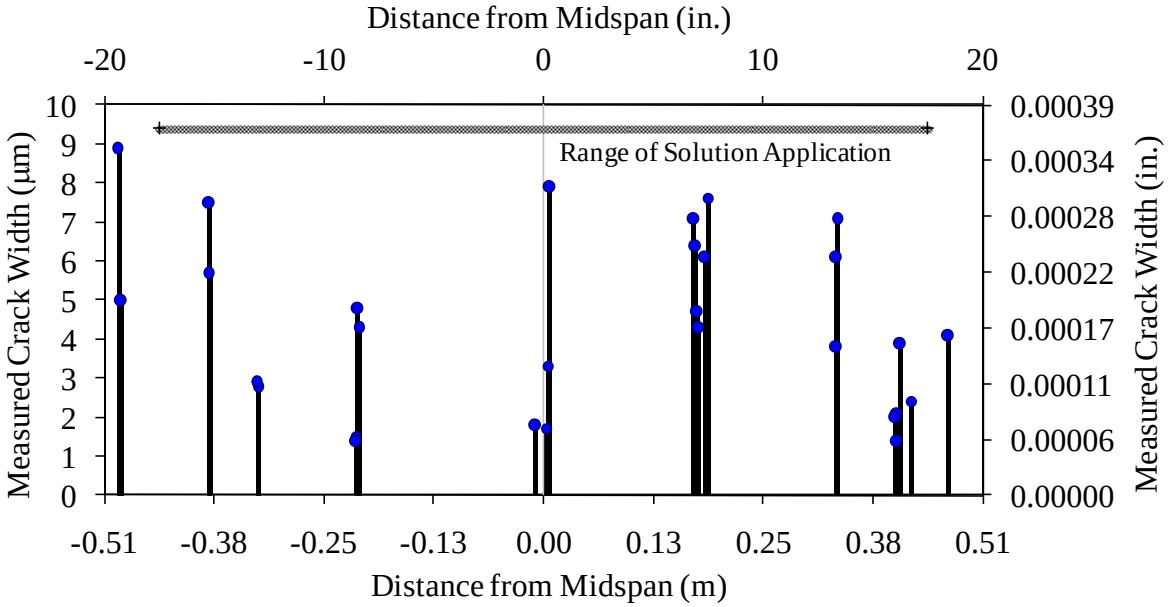

Figure 10. Graph. Crack locations and widths after 1000 cycles of flexural loading.

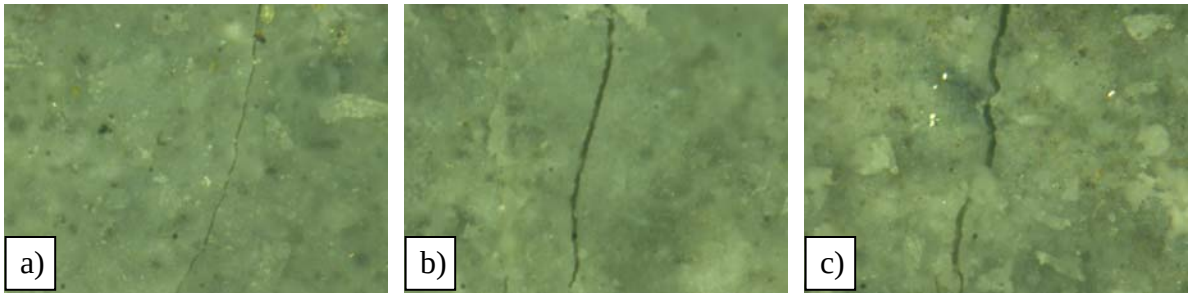

Figure 11. Photo. Photographs of a) 2-μm (0.00008-in.), b) 5-μm (0.0002-in.), and c) 8-μm (0.0003-in.) wide cracks at a magnification of 800x. The field of view of each photograph is 1.6-mm (0.063-in.) wide.

Combined Structural and Environmental Cyclic Loading

The third phase of the cyclic testing focused on the repeated application of flexural loads to the beam while simultaneously subjecting it to an aggressive environmental condition. The structural loading was continued for a total of 499,000 total loading cycles which were completed over a time period of 154 days. The aggressive environment was continuously applied to the tensile face of the beam during this entire time period.

Visual observations made during this phase of testing verified that the salt solution being applied to the bottom face of the beam was entering the flexural cracks. The photo in Figure 12, captured one hour after the start of this phase of testing, shows salt solution emanating from flexural cracks. The photo in Figure 13 shows that the salt solution migrated along and evaporated from many cracks, with salt residue being left behind. Salt residue was observed to be deposited on the face of the beam as high as 240-mm (9.5-in.) up from the bottom of the beam.

Figure 12. Photo. North face of beam near midspan one hour after the initiation of the third phase of cyclic testing.

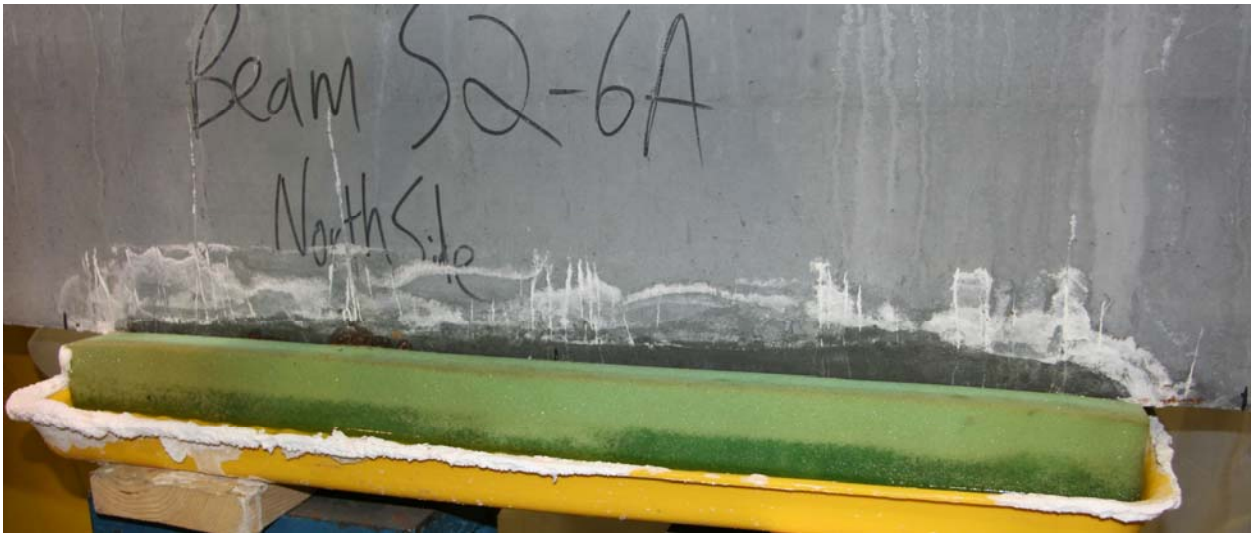

Figure 13. Photo. North face of beam near midspan immediately after the conclusion of the third phase of cyclic testing.

Actuator load and displacement data was collected periodically throughout this phase of the cyclic testing. The results previously presented in Figure 8 are expanded in Figure 14 to show the load displacement responses at twelve specific cycles ranging from first flexural cracking to the conclusion of this phase of testing. This figure demonstrates that the rate of change in flexural response decreased as the cycling progressed.

The change in flexural response was also assessed via the slope of the load-displacement response. The slope was calculated on the increasing load portion of each recorded cycle between the loads of 13.3 kN (3 kips) and 57.8 kN (13 kips). These results are plotted in Figure 15. The text in the figure also provides periodic indications of the length of time that the beam had been exposed to the aggressive environment. This plot shows that the flexural response exhibited the greatest change during the first week of cycling, exhibited some continuing degradation during the following two months, and then was relatively stable for the final approximately three months or 320,000 cycles.

The flexural cracking of the beam was assessed following the completion of the cyclic loading through the same procedure as was used previously. Figure 16 displays the pertinent information on the 23 cracks identified, while also reproducing the information previously presented in Figure 10. Crack widths for cracks identified in the present assessment are only indicated for cracks occurring outside of the area subjected to the aggressive environment. Cracks identified within the area subjected to the aggressive environment were obscured by salt residues and thus were not able to be measured.

These crack assessment results demonstrate that this phase of cyclic flexural loading resulted in additional cracking of the beam. In the assessed areas outside of the area subjected to the aggressive environment, a total of nine cracks were identified whereas only three cracks has been identified prior to this phase of loading. Also, this figure demonstrates that some previously identified cracks were not identifiable during this assessment and that new cracks were identified in previously uncracked locations. Given the difficulty in locating cracks in areas subjected to

the aggressive environment, it is likely that additional cracks beyond those noted in the figure were present during this phase of testing. Figure 17 provides three photographs of a single crack within the portion of the beam subjected to the aggressive environment. This crack, which was observed to be 2.5-μm (0.0001-in.) wide at the start of this phase of testing, could only be identified at the conclusion of this phase of testing through microscopic scanning at a wider field of view.

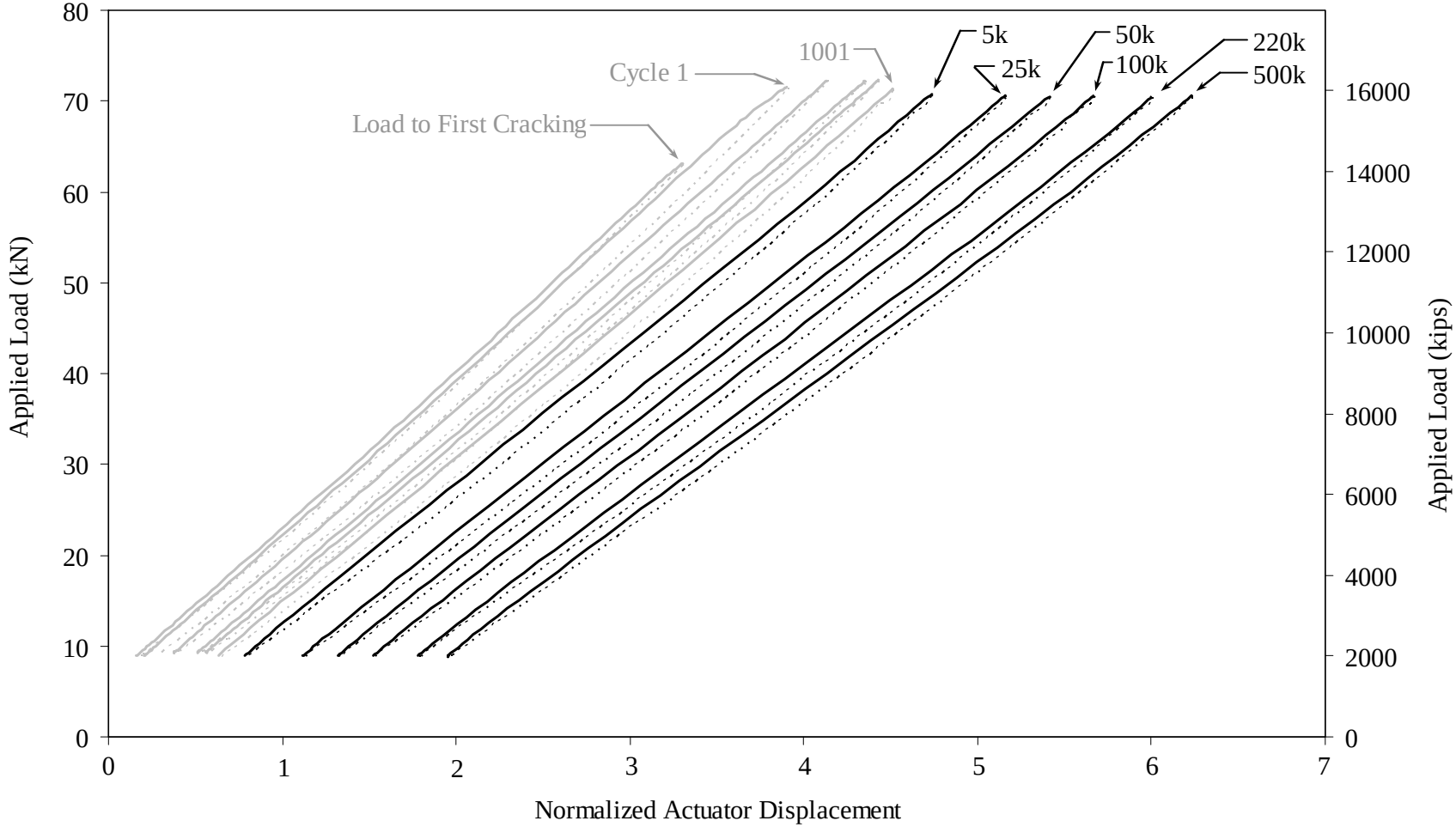

Figure 14. Graph. Actuator load versus displacement response during third phase of cyclic loading.

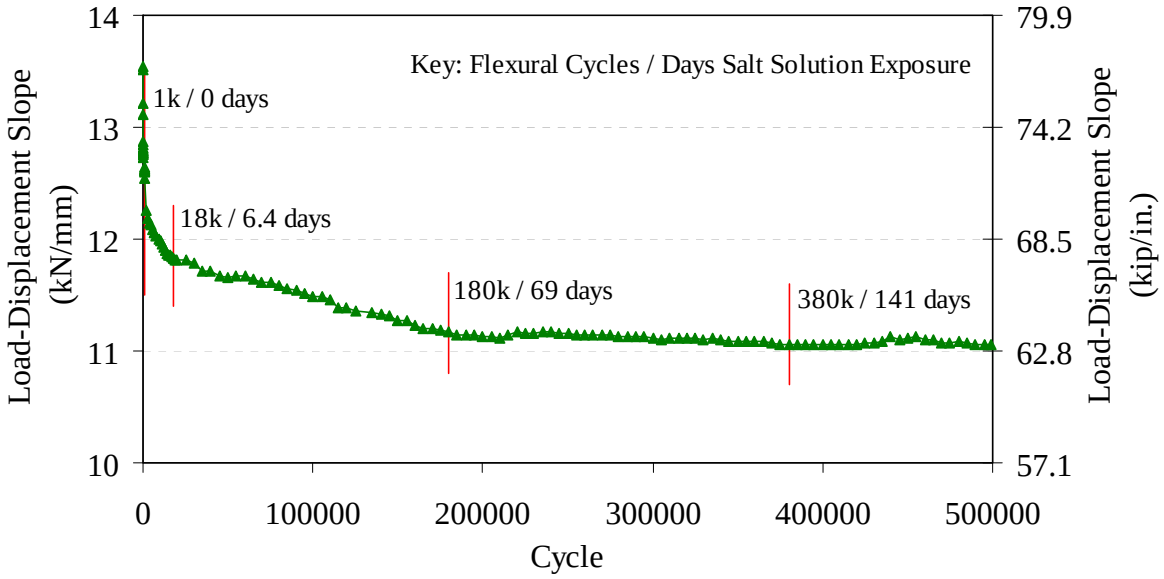

Figure 15. Graph. Actuator load-displacement response slope during cyclic loading.

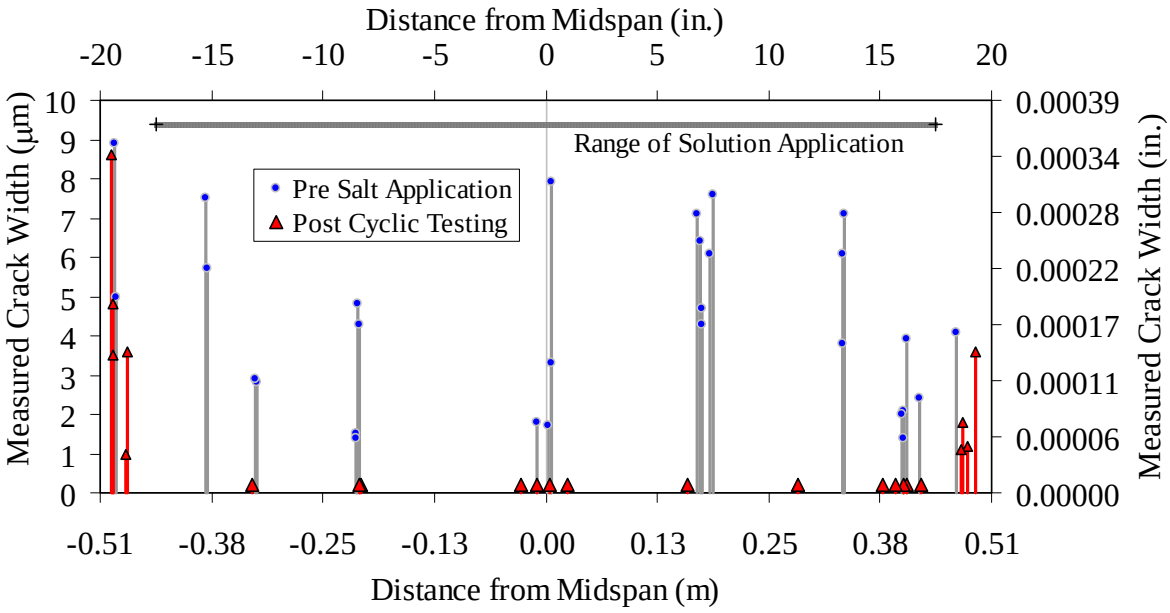

Figure 16. Graph. Crack assessment results after the conclusion of cyclic testing.

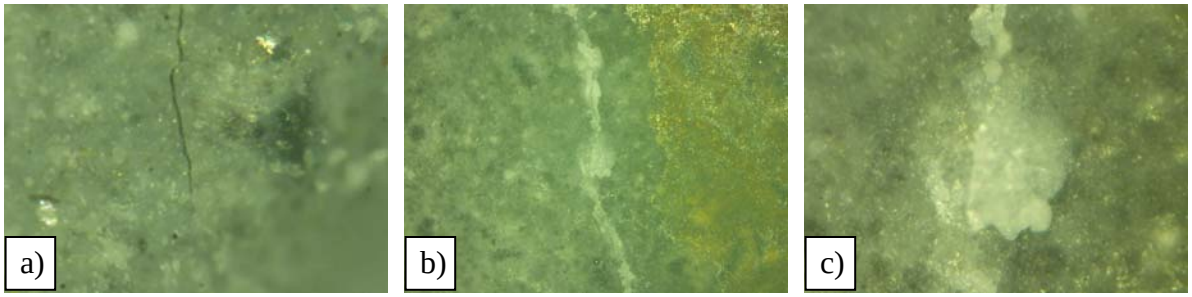

Figure 17. Photo. Photographs of a) a 2.5-μm (0.0001-in.) wide crack viewed at 800x magnification prior to salt application, and the same crack after the conclusion of cyclic testing viewed at b) 200x magnification and c) 800x magnification. The field of view of photos a) and c) is 1.6-mm (0.063-in.) wide. The field of view of photo b) is 6.4-mm (0.102-in.) wide.

Significant staining was observed on the bottom face of the beam in the region where the aggressive environment had been applied. This rust-colored staining resulted from the corrosion of steel fiber reinforcement which became exposed to the aggressive environment. Steel fibers at or just beneath the cast surface of the beam began to corrode in the presence of the concentrated salt solution and the oxygen-rich environment. Corrosion of fibers was also present on fibers exposed in a pair of small spalls which occurred during removal of the beam from the casting form. No chipping, spalling, or delaminating of the UHPC was observed to have occurred as a result of the aggressive environment to which the beam was subjected. Figure 18 provides a photograph of the bottom and north faces of the beam after the conclusion of the third phase of cyclic testing.

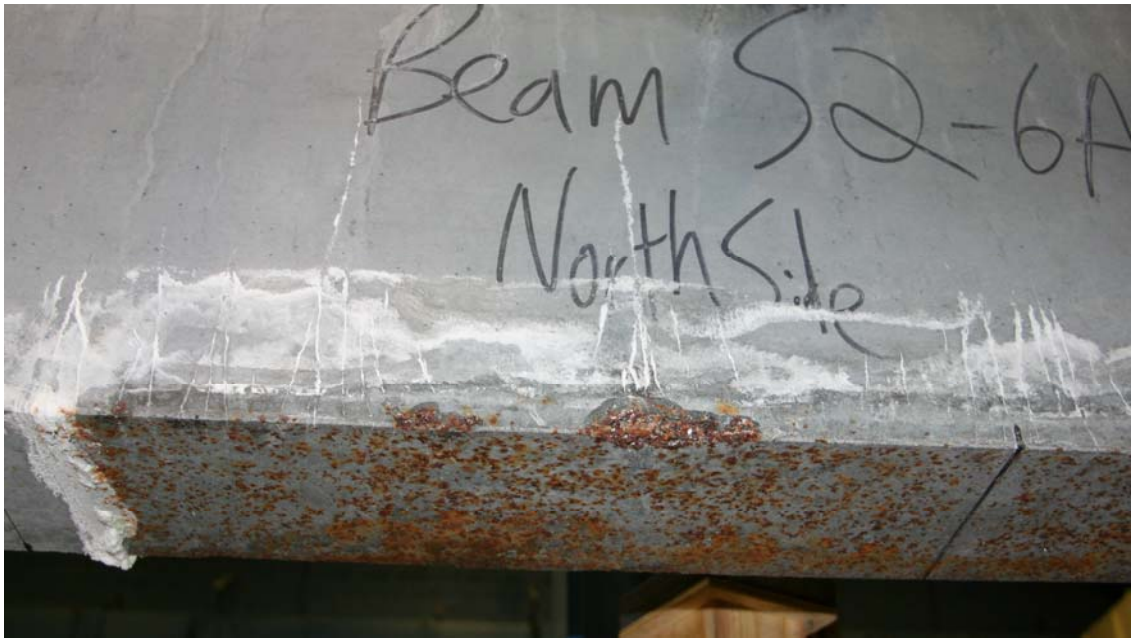

Figure 18. Photo. Bottom face and north side of beam after the conclusion of the third phase of cyclic testing.

STATIC FLEXURAL TESTING OF BEAM

Initial Test Setup and Result

Following the conclusion of the third phase of cyclic testing, the beam was subjected to a series of significant flexural loadings in an effort to assess the remaining flexural capacity of the beam and to cause the beam to fail in flexure within the area subjected to the aggressive environment. The first static flexural load application was conducted through the same structural loading setup which was used previously for the application of the structural loads. Recall that this setup included an overall beam span of 4.88 m (16 ft) and a 1.52-m (60-inch) long constant applied moment region in the center of the span. In addition to the data captured by the actuator's internal load cell and linear LVDT, an additional pair of LVDTs was attached to the midspan of the beam so as to capture the midspan vertical deflection during the load application. The beam was loaded at a continuous actuator displacement rate of 0.762 mm/minute (0.03 in./minute).

Figure 19 presents the load-deflection response of the beam. The beam exhibited a linear-elastic response until the first new flexural cracking was audibly observed at an applied load of 86.7 kN (19.5 kips). At an applied load of approximately 93.4 kN (21 kips) the load-deflection response shows a clear softening. The applied load grew until the peak was reached at 165 kN (37.1 kips) which corresponds to a total midspan moment of 143 kN-m (1265 kip-in.). This peak load signified the point in the response when the fibers crossing an individual discrete flexural crack began to debond thus allowing the initiation of the hinging of the beam. The actuator continued to push the beam for an additional 2.5 mm (0.1 in.) of midspan displacement after the peak load was reached.

The failure crack as observed after the removal of the applied load is shown in Figure 20. This crack intersected the bottom of the beam approximately 203-mm (8-in.) east of the east load point. This failure location, although outside of the constant moment region wherein the largest moment was applied, did coincide with the cross section wherein a rebar chair supported the mild steel reinforcement during casting. The flexural failure of the cross section at this location indicates that the flexural capacity of the beam was not significantly degraded by the 154 day application of the aggressive environment during the cyclic flexural loading.

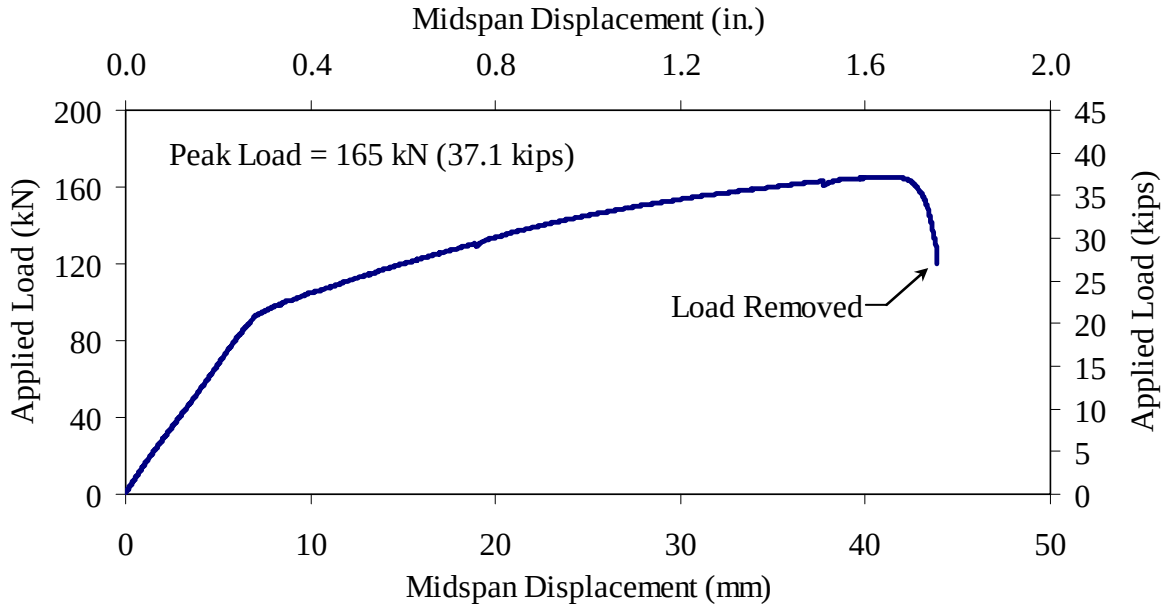

Figure 19. Graph. Load versus midspan displacement response of beam subjected to static load to failure.

Figure 20. Photo. Failure crack east of east load point.

First Subsequent Flexural Loading

The loading arrangement was modified in order to subject the central portion of the beam to additional flexural loading. The same loading frame and load application mechanisms were used; however, the spans were modified. The overall span of the beam was decreased to 1.83 m (72 in.), with the east support point located just west of the previous failure crack. The load points were still centered on the span, and the center-to-center distance between load points was decreased to 305 mm (12 in.). This loading arrangement created a four-point bending setup

wherein the constant moment region was entirely contained within the portion of the beam which was subjected to the aggressive environment. Electronic data was not collected during this loading as it was solely intended to cause the beam to fail across a pre-existing crack near midspan. Figure 21 shows the overall setup for this flexural loading.

The load was increased until the total applied load reached 302 kN (68 kips) which corresponded to a total maximum moment in the beam of 139 kN-m (1229 kip-in.). At this load, the beam displayed no indication than any individual crack was beginning to widen. This load was the maximum that could be applied through the present loading setup, thus the beam was unloaded without having achieved the desired flexural failure. This result again demonstrated a minimum flexural capacity for this beam.

Figure 21. Photo. Test setup for first subsequent flexural loading.

Second Subsequent Flexural Loading

A final effort was undertaken to force the beam to fail in flexure within the region subjected to the aggressive environment. The beam was removed from the original load frame, turned upside down, and placed into a three-point bending reaction frame. The frame included reaction tie-downs spaced at 1.83 m (72 in.) and a static hydraulic jack topped by a half-roller. The static jack was situated midway between the reaction points. The beam was placed so that the load application point was 50 mm (2 in.) toward the original west end of the beam from the original midspan location. Figure 22 shows a photograph of the test setup.

The midspan displacement imposed by the hydraulic jack was steadily increased until the beam failed in flexure. The applied load was not monitored and thus the peak applied moment was not captured. Figure 23 shows the beam after the initiation of fiber pullout and flexural failure. The flexural failure initiated within the region subjected to the aggressive environment, but was not

coincident with any cracks which existed during the application of said environment. The hydraulic jack continued to impose displacement until the rebar ruptured and the beam separated into two pieces. Figure 24 provides an elevation view of half of the failed beam. Tensile flexural failure initiated approximately 100 mm (4 in.) east of the load application point.

Figure 25 shows a photo of the tensile flexural failure surfaces, and Figure 26 provides a close-up view of one of the failure surfaces. Visual inspection of the failure surfaces provided no indication that this failure location was impacted by the presence of the aggressive solution or the flexural fatigue loading. These failure surfaces displayed no indication of fiber fatigue failure, fiber rupture, or fiber corrosion. They also did not show any indication of rebar corrosion.

Inspection of the locations where cracks generated by the cyclic portion of the study intersected with the current failure surfaces indicated that the salt solution did not penetrate a significant distance into the interior of the beam. Figure 27 provides a photo of a piece of UHPC removed from the failure region. The cast face shows salt deposits along a discrete crack. At the intersection of the cast face and the failure surface, the salt deposits can be observed to extend approximately 3 mm (0.12 in.) into the interior of the concrete.

Figure 22. Photo. Test setup for second subsequent flexural loading.

Figure 23. Photo. Beam failure near midspan after second subsequent flexural loading.

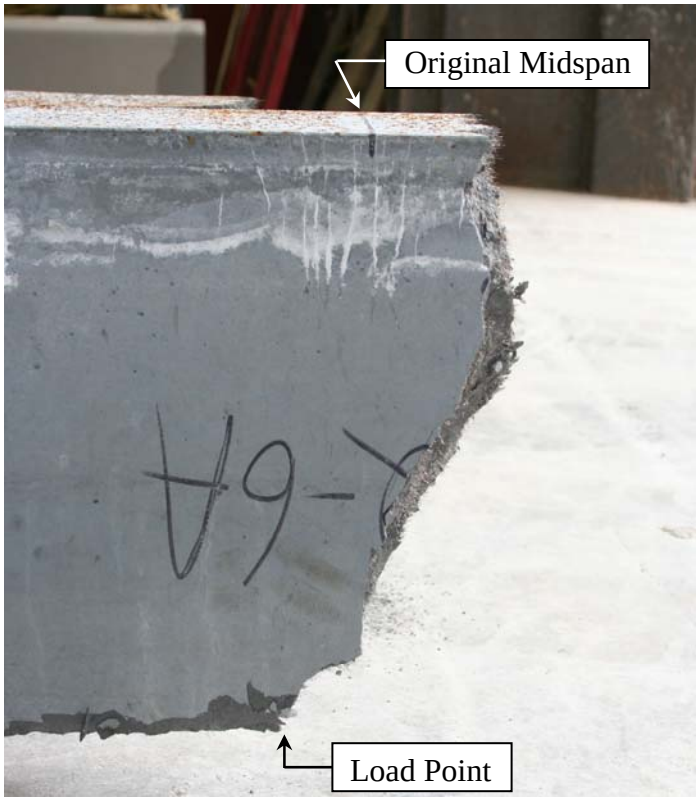

Figure 24. Photo. Elevation view of failure location.

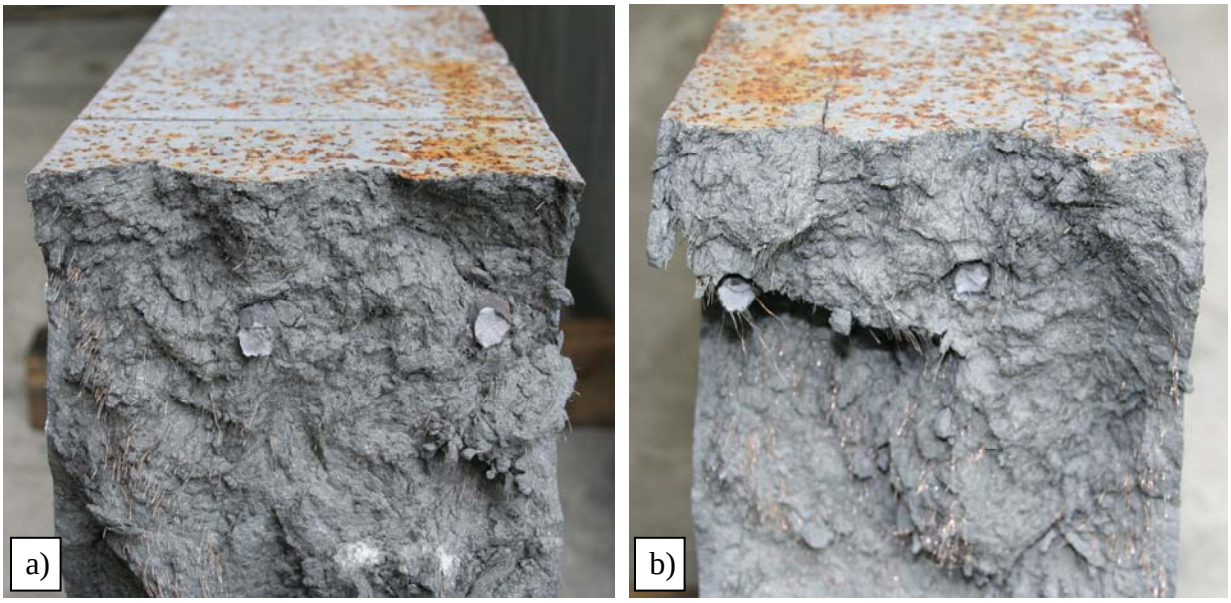

Figure 25. Photo. East and west faces of failure surface.

Figure 26. Photo. Close-up of failure surface.

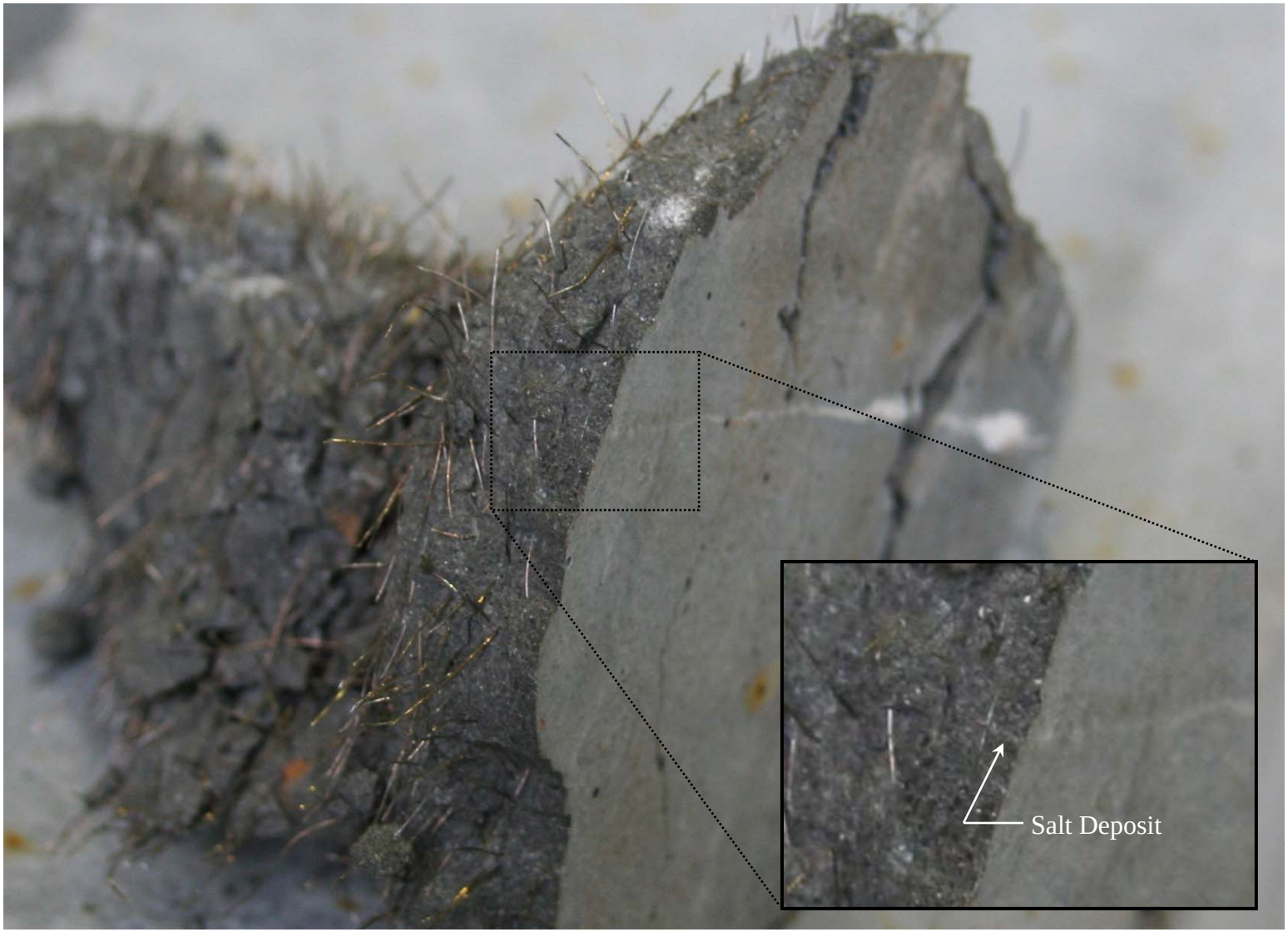

Figure 27. Photo. Intersected flexural crack showing 3-mm (0.12-in.) depth of salt penetration.

EXTRACTED COMPONENT DIRECT TENSILE TESTING

Following the flexural failure of the beam, a prism was extracted from the portion of the beam subjected to the aggressive environment. This prism was then tested in direct tension so as to assess the residual ultimate tensile strength of the UHPC.

Extraction Process and Test Setup

The prism was extracted from the tensile face of the beam near the flexural failure location. The prism was obtained through the use of a concrete saw with a diamond blade. The cutting was completed without the use of any water so as to ensure that the extraction process did not facilitate the hydration of unreacted cementitious particles on any exposed or cracked surfaces. Figure 28 shows a photo of the extraction process. The horizontal cut was completed immediately below the depth of the reinforcing bar. The dimensions of the resulting prism were 25.4 x 50.8 x 300 mm (1.0 x 2.0 x 11.9 in.), which were consistent along the length of the prism to within 1.6 mm (0.063 in.). One face of the prism was a cast face that had previously been subjected to the aggressive environment. A second face of the prism was a vertical face of the beam which was adjacent to the aggressive environment.

The prism was tested in direct tension through the use of a 500-kN (112-kip) capacity Instron uniaxial testing machine. This testing machine included flat-plate hydraulic grips for engaging two faces of the prism, thus allowing for the generation of uniaxial tensile forces in the prism through friction between the gripped ends and the machine grips. The cross-head movement was maintained at a constant 0.762 mm/minute (0.03 in./minute) displacement rate for the duration of the first two tests; 0.254 mm/minute (0.01 in./minute) was used for the third test. Applied load and cross-head displacement were monitored and captured throughout each test. Figure 29 provides two photos of the extracted prism just prior the initiation of the first direct tensile test. Note the lines of salt residue which are visible in the figure, indicating the location of cracks generated during the cyclic flexural testing.

Figure 28. Photo. Extraction of a prismatic specimen from beam tensile face.

Figure 29. Photo. Two photos of the direct tensile testing of a UHPC prism.

Test Results

Three uniaxial tensile tests were completed on the prism, with each test applying load to the longest remaining portion of the prism. Recall that the tensile behaviors of UHPC are influenced by the fiber reinforcement dispersion and orientation, both of which are favorably represented in this prism which was extracted from the bottom corner of a horizontally-cast beam element. As such, recognize that the tensile properties reported below are indicative of local uniaxial behaviors, not global bulk properties.

The first test was completed with an approximately 180-mm (7-in.) clear space between the grip faces and a uniform prismatic cross section. The load versus nondimensionalized cross-head displacement is presented in Figure 30. Note that the displacement includes various types of testing machine- and grip-related deformations not associated with the UHPC specimen, and thus it should only be viewed from a qualitative standpoint. The prism failed at a peak uniaxial stress of 12.9 MPa (1.88 ksi) based on the applied load and the cross-sectional dimension at the failure location. Figure 31 shows the prism as the fibers were beginning to pullout across the failure plane. Based on salt residue visible on the two cast faces of the prism, the tortuous failure plane crossed at least two cracks which were present during the cyclic testing. However, there was no indication that the failure plane followed the path of any preexisting cracks.

The second prism test was completed through the use of an identical testing procedure. The longer piece of the original prism was used for the test, resulting in an approximately 150-mm (3-in.) distance between the grip faces. Figure 30 again shows the stress versus cross head

displacement response. The prism failed at a peak uniaxial stress of 15.8 MPa (2.30 ksi). Figure 31 shows the prism as the fibers were beginning to pullout across the failure plane. Based on salt residue on the two cast faces of the prism, the tortuous failure plane crossed at least two cracks which were present during the cyclic testing. The failure plane followed a preexisting crack plane over a 40-mm^2 (0.062-in^2) triangular area immediately adjacent to the cast face subjected to the aggressive solution and a cut face. In this area, salt residue was noted on part of the crack face indicating that the salt solution entered at least 5 mm (0.2 in.) into the bottom face of the beam. Additionally, 25 fibers were noted to emanate from the two faces of this preexisting cracked area; corrosion staining was only observed on fibers located within 2 mm (0.08 in.) of the beam surface subjected to the aggressive solution.

The third prism test was completed through the use of the portion of the original prism which fell between the failure surfaces of the first and second prism tests. In an attempt to force the tensile failure to occur along a crack generated during the cyclic testing, a crack near the center of the prism was selected for routing. The portions of the intersection of the crack plane with the exterior of the prism which were not indicated by salt residue were marked through the use of an alcohol-based evaporative identification technique. The crack was then routed to a depth of between 1 and 1.5 mm (0.04 and 0.06 in.) around the entire perimeter of the prism. A rotary tool with a 1 mm (0.04 in.) diameter head was used to complete the routing. Once inserted into the testing machine, the exposed length of prism between the grip faces was approximately 25 mm (1 in.). Figure 32 shows this test specimen immediately prior to the initiation of testing and Figure 33 shows the crack which was routed for this test.

Figure 30 again shows the stress versus cross head displacement response. The prism failed at a peak uniaxial stress of 18.1 MPa (2.63 ksi). The failure surface intersected the routed groove around approximately 75 percent of the perimeter of the prism. However, the failure surface only followed the preexisting crack over a 20-mm^2 (0.031-in^2) area; this area was adjacent to the surface subjected to the aggressive environment. Figure 34 provides a photograph of the failed cross section with an annotation indicating the area of concurrence with the preexisting crack. Salt residue is visible on this concurrent surface which has a maximum depth of 3 mm (0.12 in.) from the exterior.

In total, these three direct tensile tests provided an indication of the minimum ultimate tensile capacity of the UHPC subjected to the aggressive environment. These results seem to indicate that there can be significant spread in the tensile strength results, with higher strengths likely to be observed when the failure is forced to initiate at a specific location. The third test, whose failure was forced to initiate near a preexisting crack, exhibited a 40 percent increase in tensile strength as compared to the first test.

The results also indicate that the aggressive environment to which the beam was subjected did not significantly reduce the tensile strength of the UHPC. The fact that none of the failure planes for the three tests significantly followed the preexisting cracks in the prisms indicates that the collective fiber reinforcement bridging the preexisting cracks must have retained a significant portion of its tensile capacity. The locations where failures followed preexisting cracks indicate that the aggressive solution entered at least 5 mm (0.2 in.) toward the interior of the beam.

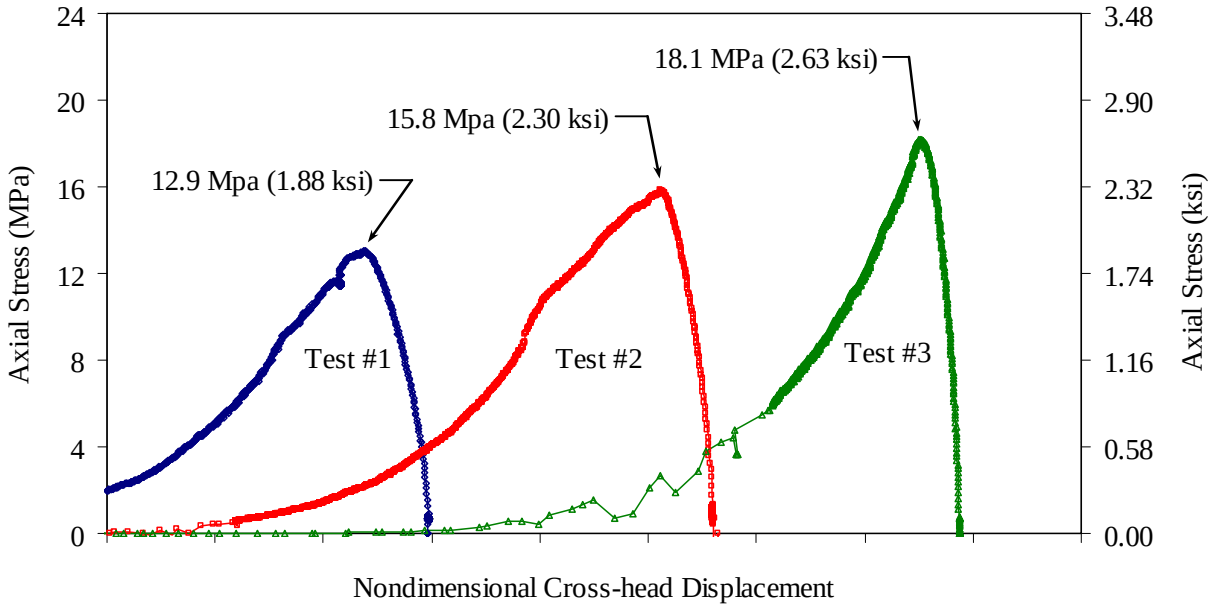

Figure 30. Photo. Stress-displacement responses from three direct tensile tests.

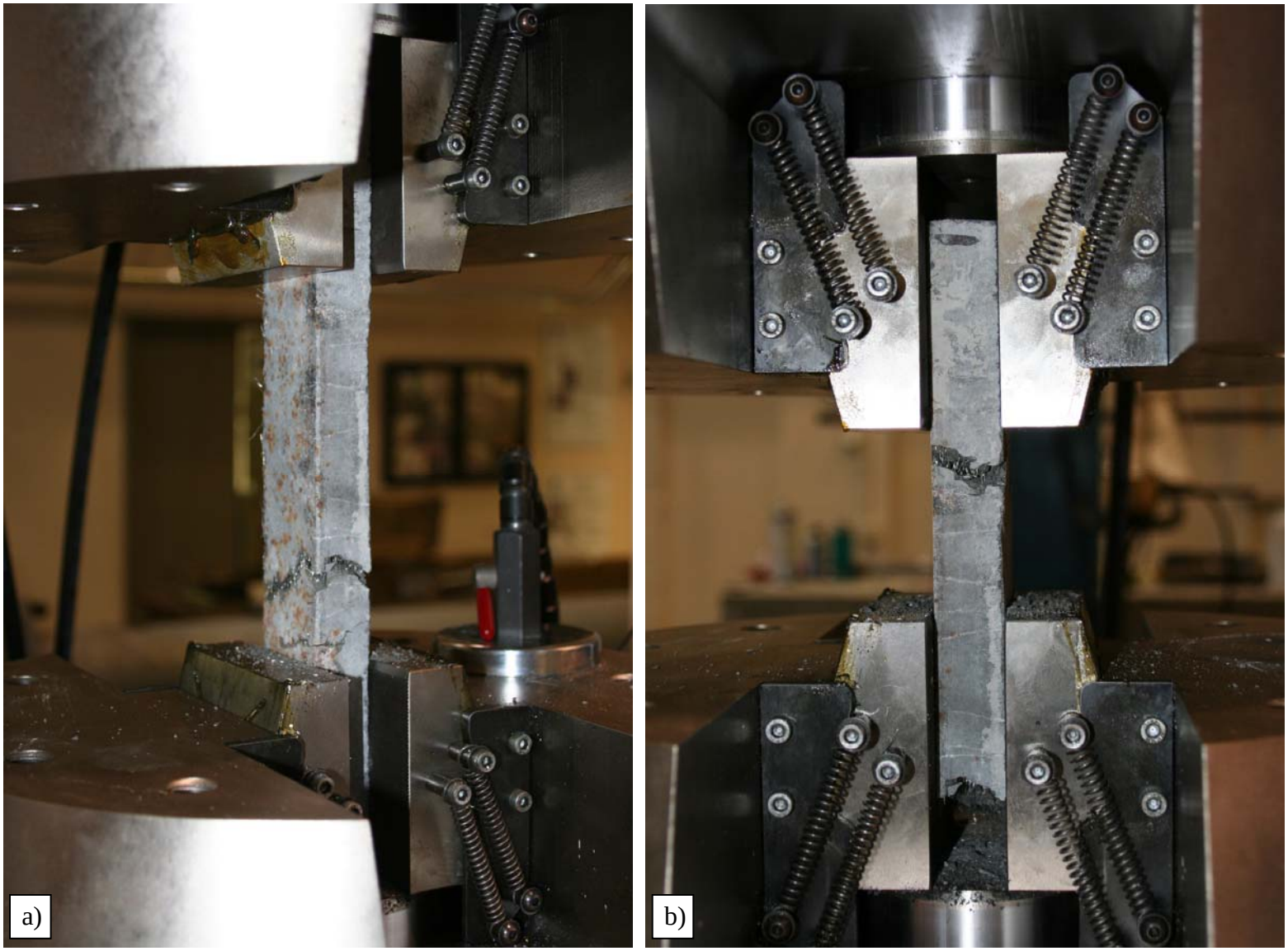

Figure 31. Photo. Strain localization and fiber pullout in a) first and b) second direct tensile tests.

Figure 32. Photo. Third direct tensile test of a UHPC prism.

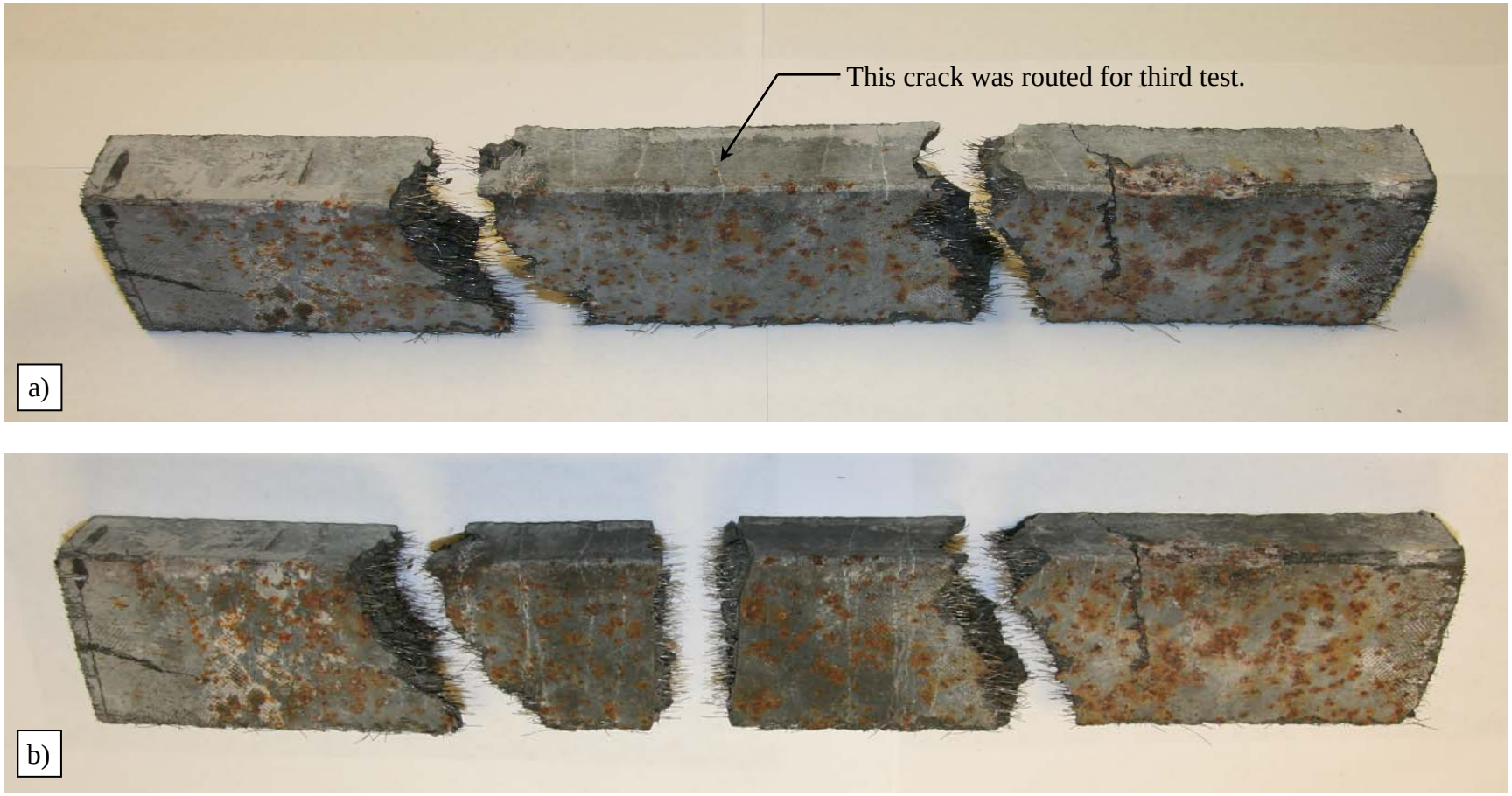

Figure 33. Photo. Failed UHPC tensile prism after a) second test and b) third test.

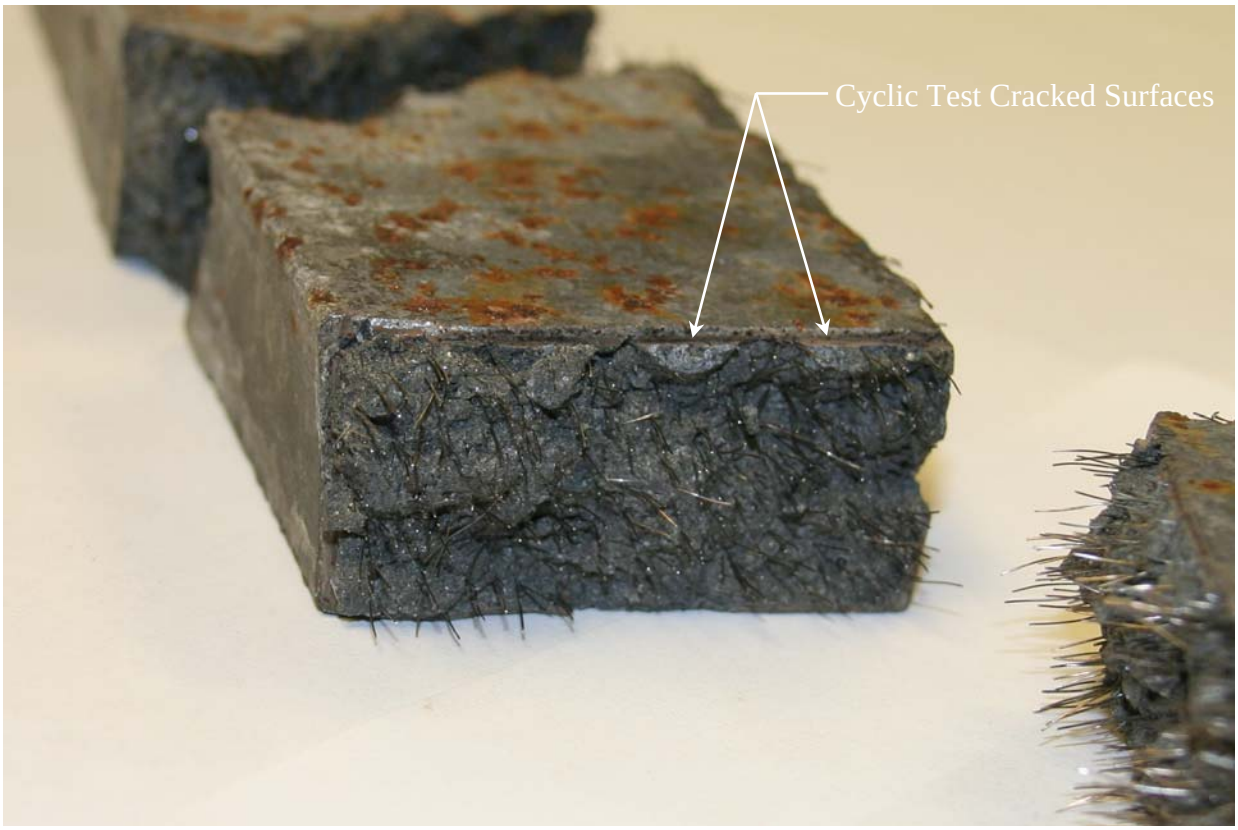

Figure 34. Photo. Failure surface after the conclusion of the third direct tensile test.

CHAPTER 5. CONCLUSIONS

INTRODUCTION

This experimental investigation focused on the flexural performance of a UHPC component subjected to a simultaneous combination of structural loading and aggressive environmental conditions. This loading combination is commonly present in transportation structures subjected to frequent transient loads and deicing chemicals. Given the homogeneity and exceptionally low permeability of uncracked UHPC, it is anticipated that discrete structural cracking in UHPC components would necessarily increase the permeability. Any ingress of liquids into the UHPC component along crack faces raises the possibility of steel fiber reinforcement degradation and a resulting loss of UHPC tensile capacity. The objective of this research program was to evaluate the tensile response of UHPC under these conditions in order to assess whether degraded tensile performance resulted. Conclusions resulting from this study are presented below. A brief discussion of ongoing and potential future research related to this topic is presented immediately thereafter.

CONCLUSIONS

The following conclusions are presented based on the research presented in this report.

1. The simultaneous application of structural and environmental loadings to a UHPC flexural member did not result in any apparent degradation of the member's flexural capacity. The aggressive environmental load consisted of the application of a 15% NaCl solution on the tensile face of the beam. The structural loading consisted of the application of four-point bending load which surpassed the load which caused first flexural tensile cracking by 14%. The structural and environmental loading was conducted for 154 days during which 500,000 cycles were applied.

2. The open-cell sponge was an effective method of applying the 15% NaCl solution to the tensile face of the beam. The compression of the sponge during each structural load cycle caused the solution to be applied to the face of the beam. The solution migrated up the cross section within the flexural tensile cracks and was observed to evaporate from crack surfaces on the vertical face of the beam.

3. Tensile cracking of UHPC is indicative of cementitious matrix properties, and is not necessarily indicative of a plane wherein tensile failure of the section through fiber pullout will eventually occur. In one four-point bending test, one three-point bending test, and three discrete uniaxial tension tests, the failure plane where fiber pullout occurred at ultimate tensile capacity did not coincide with the initially cracked planes generated and subjected to loading during the cyclic phase of testing.

4. Uniaxial tensile testing of prismatic UHPC specimens is a viable means of assessing the tensile behaviors of this fiber reinforced concrete. A prismatic section was extracted from the aggressively loaded tensile face of the UHPC, was clenched between the hydraulic grips of a uniaxial testing machine, and was loaded in direct tension. Three

discrete tests to failure were completed on an individual prism, each time with a decreased gage length.

5. Reducing the cross sectional area of a uniaxial tensile specimen at a preexisting crack will not necessarily force the specimen to fail across said crack. Structural cracking planes in UHPC tend to be comparatively flat, while ultimate tensile capacity failure planes are tortuous. Fiber pullout, which defines the ultimate tensile capacity, presumably occurs at locations wherein the combination of the resistances provided by the cementitious matrix and the fiber reinforcement are insufficient to carry the applied load. Results from this test program indicate that this behavior depends significantly on the orientation and distribution of fiber reinforcement.

6. UHPC can exhibit a wide range of ultimate tensile capacities within a small portion of an individual specimen. Cross sections along a 180-mm (7-in.) length of an individual prism were observed to fail at 12.9 MPa (1.88 ksi), 15.8 MPa (2.30 ksi), and 18.1 MPa (2.63 ksi). These stresses represent minimum capacities over finite gage lengths in the first two cases, and represent the capacity at a predisposed cross section in the third case.

7. The application of the structural and environmental loading was not observed to cause any local degradation of the fiber reinforcement bridging cracked planes. Ingress of NaCl solution toward the interior of the beam within cracked planes was only observed to a depth of 3 mm (0.12 in.) on the side face of the beam. Direct application of the NaCl solution on the tensile face of the beam served to cause the solution to penetrate at least 5 mm (0.2 in.) toward the interior of the beam. At locations where fiber pullout occurred across preexisting cracked planes, the fiber reinforcement did not shown any visible signs of tensile failure or section loss.

ONGOING AND FUTURE RESEARCH

The results of this study demonstrate that UHPC can retain its tensile capacity under aggressive environmental conditions and cyclic structural loading. A related study is currently being initiated to quantitatively assess the permeability of UHPC previously subjected to structural loads exceeding the elastic limit of the cementitious matrix. This study will use test specimens extracted from structural components in combination with non-reactive liquids of similar viscosity to water to assess the potential increased liquid ingress that can occur due to cracking.

A second study focused on assessing the technical and practical aspects of uniaxial tensile testing of UHPC prismatic sections is in development. Existing methods of assessing the tensile mechanical properties of UHPC have many shortcomings. The tensile testing method described in the present study provides a direct assessment of pre- and post-cracking tensile behavior from load initiation through to ultimate capacity and fiber pullout. Additionally, it can be completed on extracted or cast specimens using testing equipment commonly available in the structural materials testing industry.

REFERENCES

1. Graybeal, B., "Material Property Characterization of Ultra-High Performance Concrete," Federal Highway Administration, Report No. FHWA-HRT-06-103, August 2006, 186 pp.
2. Graybeal, B., "Structural Behavior of Ultra-High Performance Concrete Prestressed I-Girders," Federal Highway Administration, Report No. FHWA-HRT-06-115, August 2006, 104 pp.
3. Graybeal, B., "Structural Behavior of a Prototype Ultra-High Performance Concrete Pi-Girder," Federal Highway Administration, National Technical Information Service Accession No. PB2009-115495, November 2009, 145 pp.
4. Graybeal, B., "Structural Behavior of a 2nd Generation Ultra-High Performance Concrete Pi-Girder," Federal Highway Administration, National Technical Information Service Accession No. PB2009-115496, November 2009, 113 pp.
5. Meade, T., and B. Graybeal, "Flexural Response of Lightly Reinforced Ultra-High Performance Concrete Beams," *Proceedings, 3rd fib International Congress*, Washington, D.C., May 30 – June 2, 2010, 17 pp.
6. Gérard, B., S. Jacobsen, and J. Marchand, "Concrete Cracks II: Observation and Permeability – A Review," Concrete Under Severe Conditions 2: Environment and Loading, Volume 1, pp. 183-197.
7. Reinhardt, H-W., M. Sosoro, and X-F. Zhu, "Cracked and Repaired Concrete Subject to Fluid Penetration," *Materials and Structures*, V. 31, March 1998, pp. 74-83.
8. Wang, K., D. Jansen, and S. Shah, "Permeability Study of Cracked Concrete," *Cement and Concrete Research*, V. 27, No. 3, 1997, pp. 381-393.
9. ASTM C39, "Standard Test Method for Compressive Strength of Cylindrical Concrete Specimens," American Society for Testing and Materials Standard Practice C39, Philadelphia, PA, 2001.
10. Graybeal, B., "Practical Means for the Determination of the Tensile Behavior of Ultra-High Performance Concrete," *Journal of ASTM International*, V. 3, No. 8, December 2006, 9 pp.
11. ASTM C496, "Standard Test Method for Splitting Tensile Strength of Cylindrical Concrete Specimens," American Society for Testing and Materials Standard Practice C496, Philadelphia, PA, 2002.
12. ASTM A370, "Standard Test Methods and Definitions for Mechanical Testing of Steel Products," American Society for Testing and Materials Standard Practice A370, Philadelphia, PA, 1997.
13. Association Française de Génie Civil, *Interim Recommendations for Ultra High Performance Fibre-Reinforced Concretes*, 2002.
14. Pansuk, W., H. Sato, Y. Sato, and R. Shionaga, "Tensile Behaviors and Fiber Orientation of UHPC," *Proceedings, Second International Symposium on Ultra High Performance Concrete*, March 5-7, 2008, Kassel, Germany, pp. 161-168.

15. Kim, S., S. Kang, J. Park, and G. Ryu, “Effect of Filling Method on Fibre Orientation & Dispersion and Mechanical Properties of UHPC,” *Proceedings, Second International Symposium on Ultra High Performance Concrete*, March 5-7, 2008, Kassel, Germany, pp. 185-192.